Mechanism Behind Streptococcus Toxic Shock-like Syndrome Onset —Immune Evasion and Bacterial Properties—

Tadayoshi IKEBE[1], Manabu ATO[2], Kazuo KOBAYASHI[2] & Haruo WATANABE[1]
[1]Department of Bacteriology and [2]Department of Immunology, National Institute of Infectious Diseases

Streptococcal toxic shock-like syndrome (STSS) was firstly reported in 1987 in the United States. Japan's first definitive STSS case was reported in 1992, with over 500 cases since confirmed. Mortality is extremely high at 40%. Pathological findings, bacteria aggregation, and a paucity of polymorphonuclear neutrophils (PMN) in the foci of invasive group A streptococcal (GAS) infection suggest that host defense disturbance plays an important role in invasive infection onset. GAS, clinically isolated from severely invasive, but not from non-invasive, infections, could compromise human PMN functions in at least two independent ways-by inducing necrosis to PMN by enhanced production of pore-forming toxin streptolysin O (SLO) and by PMN migration impairment via digesting interleukin-8, a PMN attracting chemokine, through increased serine protease ScpC production. Expression of these genes was upregulated by a loss of repressive function with the *csrS* gene mutation of the two-component sensor/regulator system.

平成21年9月20日

国内発生している致死率の高い感染症①

劇症型溶血性レンサ球菌感染症

池辺 忠義

劇症型溶血性レンサ球菌感染症(streptococcal toxic shock syndrome)は1987年に米国で最初に報告され，その後，先進国ばかりでなく，発展途上国からも報告されている．日本における最初の典型的な症例は1992年に報告されており，現在までに500人を超える患者が確認されている．そして，このうち約30%が死亡しているというきわめて致死率の高い感染症である．A群レンサ球菌感染による一般的な疾病は咽頭炎であり，その多くは小児が罹患する．一方，劇症型溶血性レンサ球菌感染症は大人から子どもまで広範囲の年齢層に発症するが，特に30歳以上の大人に多いのがひとつの特徴である．

原因菌の特徴

劇症型溶血性レンサ球菌感染症は，β溶血を示す溶血性レンサ球菌により引き起こされる致死率の高い感染症である．主な原因菌である*S. pyogenes*はグラム陽性の球菌で，レンサ球菌という名前のとおり連鎖状の配列を取る．鞭毛を有していなく，芽胞を形成しない．カタラーゼ陰性である．Rebecca Lancefieldにより見出された群別で，Lancefield群別がある．この，Lancefield群別は，菌体の細胞壁に存在する多糖体抗原の免疫学的差異によりA群からZ群(I群およびJ群は除く)(W群からZ群は暫定的)まで分類されている．*S. pyogenes*は，Lancefield群別のA群に該当する．このことから，*S. pyogenes*はA群レンサ球菌と呼ばれることがある．近年では，A群以外にも，B，C，G群レンサ球菌でも引き起こされることが報告されている[1~3]．*S. pyogenes*は，血液寒天培地上で完全な溶血環を生じるβ溶血または不完全な溶血で顕微鏡的には集落の周辺に赤血球の残存を部分的にとどめるα'溶血を示す直径0.5 mm以上のコロニーを形成する．この*S. pyogenes*には数多くの表層抗原因子が知られている．このうちMタンパクは，現在100を超える菌型があり，菌の疫学マーカーとしてよく用いられているが，宿主細胞への付着や抗貪食作用を持つ病原因子のひとつでもある．また同時に，感染防御抗原としても重要な機能を果たしている．*S. pyogenes*は，劇症型溶血性レンサ球菌感染症を引き起こすこと以外に，一般的にはヒトの気道粘膜や皮膚から空気中に散布され，皮膚，粘膜から進入して咽頭炎，猩紅熱，膿皮症，丹毒，急性リウマチ熱，急性糸球体腎炎などの様々な疾患の原因菌として知られている．

*S. pyogenes*の病原因子は，他の細菌と比べ非常に多彩であるとともに，*S. pyogenes*の中でも保有している病原性因子が菌株により異なる．接着因子として，フィブロネクチン結合タンパク質，ラミニン結合タンパク質，Mタンパクなどが知られており，これらは，粘膜上皮や細胞外マトリクスなどに接着するときに重要な役割を示すことが知られている．細胞障害に関与するものとして，ストレプトリジンOやストレプトリジン

いけべ ただよし：国立感染症研究所細菌第一部　連絡先：〒162-8640 東京都新宿区戸山1-23-1

S, NADアーゼなどが知られている．ストレプトキナーゼは，線溶系を活性化し，血液凝固を阻止する因子として知られている．タンパク分解酵素の中には，システインプロテアーゼであるSpeB，補体であるC5aやC3を分解するC5aペプチダーゼ，C3プロテアーゼ，IL-8分解酵素であるScpC/SpyCEPなどがある．この他の分解酵素として，抗体を分解するEndoSやMac/IdeSなどが知られている．Sicタンパク質は，補体阻害因子として機能する．さらに，T細胞活性化因子として，SpeA，SpeC，SpeG，SpeH，SpeI，SpeJ，SpeK，SpeL，SpeMなどのスーパー抗原も知られている．

劇症型/重症溶血性レンサ球菌感染症患者分離株の症状

劇症型溶血性レンサ球菌感染症は，罹患者が重篤な基礎疾患を持っていないにもかかわらず，突然発病する場合がある．初期症状としては，四肢の疼痛，腫脹，発熱，血圧低下などで，発病から病態の進行が非常に急激かつ劇的で，いったん発病すると数十時間以内には急性腎不全，成人型呼吸窮迫症候群(ARDS)，播種性血管内凝固症候群(DIC)，多臓器不全(MOF)，軟部組織壊死を引き起こし，患者をショック症状から死に至らしめる．妊産婦における症例も報告されている[4]．

Stevensら[5,6]の報告によると，劇症型溶血性レンサ球菌感染症の最も一般的な初期症状は急激に始まる四肢の疼痛であり，その部位の圧痛を示す．疼痛は，通常，四肢で見られる．疼痛の開始前に，約20%の患者では，発熱，悪寒，筋肉痛，下痢のようなインフルエンザ様の症状を示す場合がある．臨床所見として，発熱が最も一般的な徴候である(ただし，患者の10%では発見時にすでにショックによる低体温を示す例がある)．錯乱状態(confusion)は患者の55%で見られ，患者によっては，昏睡や好戦的な姿勢を示すことがある．局所的な腫脹，圧痛，疼痛，紅斑のような軟部組織感染の徴候は，皮膚の傷口が存在する場合によく見られる．発熱を持つ患者で紫色の水疱が圧痛のある部位に見られると，筋炎や壊死性筋膜炎のような深部の軟部組織感染を起こしている可能性が考えられる[7]．Stevenら[5]の報告によると，劇症型溶血性レンサ球菌感染症の患者の約35%は皮膚(minor trauma, surgical procedures, intravenous drug abuse)，あるいは約20%は粘膜(pharynx, vagina)からの*S. pyogenes*の感染であり，残りの約45%は，正確な菌の侵入部位が不明である．

1999年4月に施行された「感染症の予防及び感染症の患者に対する医療に関する法律(感染症法)」による集計によると，2000年には45例，2001年には43例，2002年には90例，2003年には52例，2004年には53例，2005年には60例が報告されている．2006年の法の改正で，劇症型溶血性レンサ球菌感染症の届出基準が一部変更され，今まで起因菌をA群レンサ球菌に限定していたが，この改正でβ溶血を示すレンサ球菌にまで広げられた．感染症法に基づく医師および獣医師の届出は，以下のホームページに記載されている(http://www.mhlw.go.jp/bunya/kenkou/kekkaku-kansenshou11/01-05-06.html)．改正後，年間約100例が報告されている(2006年107例，2007年96例，2008年111例)．

2009年9月30日までに衛生微生物技術協議会溶血性レンサ球菌レファレンスシステムセンター(**表**)に集められたA群溶レン菌による劇症型/重症溶血性レンサ球菌感染症389例中，ショックは81.5%(317症例)，腎障害は60.9%(237症例)，播種性血管内凝固症候群(DIC)は61.4%(239症例)，肝障害は45.2%(176症例)，成人型呼吸窮迫症候群(ARDS)は26.0%(101症例)，紅斑様皮膚発赤疹は16.2%(63症例)，軟部組織壊死(壊死性筋膜炎および筋炎を含む)は69.4%(270症例)，中枢神経症状は32.1%(125症例)の頻度で見られた．患者の年齢は，0歳から99歳と幅広いが，30代から80代に多い．その中でも60代が最も多く，24.6%を占める(**図**)．平均年齢は，52.5歳(発症年齢0～99歳)である．性別は，男性53.2%，女性46.8%であり，性別による差は見られなかった．

特集

表　衛生微生物技術協議会溶血性レンサ球菌レファレンスシステムセンター窓口

A群レンサ球菌のT, M型別試験，および劇症型A群レンサ球菌感染症に関する情報についての窓口は以下の機関になっておりますので，お問い合わせをお願いいたします．

●センター
国立感染症研究所　細菌第一部
〒162-8640　東京都新宿区戸山1-23-1
tel：03-5285-1111　fax：03-5285-1163

●北海道・東北・新潟ブロック支部センター
福島県衛生研究所　微生物課
〒960-8560　福島県福島市方木田字水戸内16-6
tel：024-546-8047　fax：024-546-8364

●関東・甲信静ブロック支部センター
神奈川県衛生研究所　微生物部
〒253-0087　神奈川県茅ヶ崎市下町屋1-3-1
tel：046-783-4400　fax：046-783-4457

●東海・北陸ブロック支部センター
富山県衛生研究所　細菌部
〒939-0363　富山県射水市中太閤山17-1
tel：0766-56-8142　fax：0766-56-7326

●近畿ブロック支部センター
大阪府立公衆衛生研究所　感染症部
〒537-0025　大阪府大阪市東成区中道1-3-69
tel：06-6972-1321　fax：06-6972-0772

●中国・四国ブロック支部センター
山口県環境保健センター保健科学部
〒753-0821　山口県山口市葵2-5-67
tel：083-922-7630　fax：083-922-7632

●九州ブロック支部センター
大分県衛生環境研究センター微生物担当
〒870-1117　大分県大分市高江西2-8
tel：097-554-8980　fax：097-554-8987

●東京都支部センター
東京都健康安全研究センター微生物部
〒169-0073　東京都新宿区百人町3-24-1
tel：03-3363-3231　fax：03-3368-4060

劇症型/重症溶レン菌感染症患者分離株の分子疫学

S. pyogenes には，数多くの表層抗原因子が知られている．このうちMタンパクは，耐熱性，トリプシン感受性，型特異的であり，100以上の型が知られていることから[8]，菌の疫学マーカーとしてよく用いられている．Mタンパクは，抗オプソニン作用[9,10]を有し，細胞への接着にも関与しており，病原因子として知られている．分離株のM型別を行うことは病因との関連を知る上で重要であるが，継代による蛋白の脱落が生じることや市販血清がないことから，M型別の実施は困難であり，一部の機関でのみ行われている．近年，M型別を血清学的方法ではなく，M蛋白遺伝子(*emm*)の特異領域の多様性を利用し，型別する試みもなされている[11]．M蛋白質はN末より超可変領域(hypervariable region)，可変領域(variable region)，保存領域(conserved region)に分けられる．PCRに用いる2つのプライマーをデザインする場合，その1つはC末のconserved regionの各型に共通な塩基配列を用いるが，もう一方に相応するN末はhypervariable regionなので，各型に共通な配列が存在しないことから，各菌株に共通なプライマーを設定できない．M蛋白質は菌体外に突出した蛋白質であることから，菌体内で作られたときはそのM蛋白質を菌体外に分泌するためのシグナルペプチドが存在する．このシグナルペプチドはN末からbasic region，hydrophobic region，cleavage regionに分けられ，その中でもbasic regionには各型に共通な配列が存在する．したがって，シグナルペプチドのbasic regionをもう1つのプライマーに設定することができる．その2つのプライマーを用いることにより，*emm* 遺伝子の増幅が可能となる．この増幅産物の塩基配列を決定することで，遺伝子による型別が可能となった．

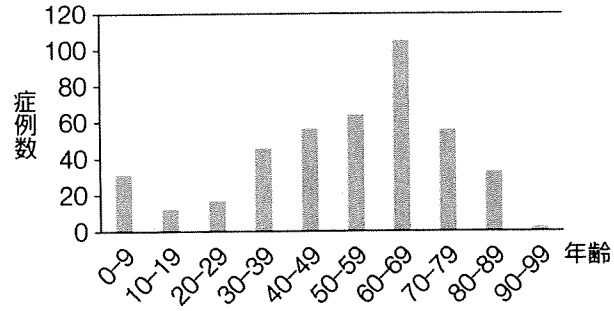

図　劇症型溶血性レンサ球菌感染症患者の年齢

2009年9月30日までに衛生微生物技術協議会溶血性レンサ球菌レファレンスシステムセンター(**表**)に集められた劇症型/重症溶レン菌感染症患者分離株408株について，*emm* 遺伝子型を調べたところ，最も多い型は，*emm1* 型で，45.3%

(185株)を占める．続いて*emm3*型(10.3%)，*emm28*型(8.1%)である．劇症型溶血性レンサ球菌感染症患者から分離される*S. pyogenes*の*emm*型は，1992～1995年までは，*emm3*型と*emm1*型が主であったが，1995年以降，*emm3*型は減少し，*emm1*型が主流となっている[12,13]．また，近年は*emm1*，*emm3*以外の型の菌も多く分離されてきているのが特徴である[14]．国立感染症研究所細菌第一部で型別した劇症型/重症溶血性レンサ球菌感染症患者由来の*S. pyogenes*は，全体で28種類にも及んでいる．

検査法

特に敗血症，四肢や体幹の激しい疼痛，発熱などを伴う患者を診た場合には，劇症型溶血性レンサ球菌感染症を鑑別診断のひとつに考える必要がある．

劇症型溶血性レンサ球菌感染症の場合には，通常無菌的である部位(血液，脳脊髄液，胸水，腹水，生検組織，手術創など)からA群レンサ球菌が検出される．特に，顕著な菌血症を示すので，血液のグラム染色標本を検鏡するとレンサ球菌が直接観察される．分離培地には血液寒天培地を用い，A群レンサ球菌はこの培地上でβ溶血またはα′溶血を示す直径0.5 mm以上のコロニーを形成する．血清群別，糖分解試験等の生化学的性状試験や検査キットにより，A群レンサ球菌であることを同定する．

劇症型溶血性レンサ球菌感染症は，病態の進行が急激であるため，早期の診断が重要である．先程述べたように，A群レンサ球菌が無菌部位から検出されることが確定診断の1つの項目となっている．血液培養の結果を待っていると，手遅れになる場合がある．近年，亜硝酸により菌の多糖体を抽出し，A群レンサ球菌を迅速に検出するキットが市販されている．血清や膿を検体として用いたとき，市販のA群レンサ球菌迅速診断キットと反応することから，この迅速診断キットが劇症型溶血性レンサ球菌感染症の診断に有用であることが報告されている[15]．また，末梢血塗末標本または壊死軟部組織の検鏡によるレンサ球菌の確認も有用である．

治療法と予防法

劇症型溶血性レンサ球菌感染症の治療には，抗菌薬としてはペニシリン系薬が第一選択薬である．また，組織内の菌密度が上昇すると菌の発育が抑制され，β-ラクタム系薬の効果が低下する現象が知られており，劇症型溶血性レンサ球菌感染症のように極端な敗血症病態を示す場合では，細胞内移行性の高いclindamycinを推奨する意見もある[16]．診断が確定したら，アンピシリン12 g/日を6時間ごととクリンダマイシン1,200 mg/日分四の投与を速やかに開始することが推奨されている[15]．さらに免疫グロブリン製剤の効果も報告されている[17]．

血圧維持には大量の輸液が必要であるが，輸液の許容範囲が狭いため，肺動脈圧の経時的観察が必要である．壊死に陥った軟部組織は菌の生息部位であり，筋壊死による腎不全および代謝性アシドーシスの悪化を防止するため，可及的広範囲に病巣を切除することが必要である[15]．

A群レンサ球菌による感染の拡散は，特に，咳やくしゃみをした後，および食事を準備する前や食べる前に，手をよく洗うことにより減らすことができる．傷口はすべて消毒して清潔に処置しておくべきであり，傷部位が赤色，腫脹，排膿および疼痛のような，感染の徴候が見られる場合には，適切に医療処置を行う必要がある．

文　献

1) Chang B, et al : Surveillance of Group B streptococcal toxic shock-like syndrome in nonpregnant adults and characterization of the strains in Japan. Jpn J Infect Dis **59**(3) : 182-185, 2006
2) Ikebe T, et al : Surveillance of severe invasive group G streptococci infections and molecular typing of the isolates in Japan. Epidemiol Infect **132**(1) : 145-149, 2004
3) Hashikawa S, et al : Characterization of group C and G streptococcal strains that cause streptococcal toxic shock syndrome. J Clin Microbiol **42**(1) : 186-192, 2004
4) 宇田川秀夫・他：A群溶連菌の激烈な敗血症により双胎胎児と母親が突然死した症例．感染症学雑誌 **67**

(12) : 1219-1222, 1993
5) Stevens DL, et al : Reappearance of scarlet fever toxin A among streptococci in Rocky Mountain West ; severe group A streptococcal infections associated with a toxic shock-like syndrome. N Engl J Med **321** (1) : 1-7, 1989
6) Stevens DL : Invasive group A streptococcus infections. Clin Infect Dis **14** (1) : 2-13, 1992
7) Stevens DL : Streptococcal infections of skin and soft tissue. In Atlas of Infectious Diseases (Stevens DL, Mandell GL, ed). 3.1-3.11, Churchill Livingstone, New York, 1995
8) Centers for Disease Control and Prevention Homepage. *Streptococcus pyogenes* database. http://www.cdc.gov/ncidod/biotech/strep/strepindex.html
9) Horstmann RD, et al : Antiphagocytic activity of streptococcal M protein ; selective binding of complement control protein factor H. Proc Natl Acad Sci USA **85** (5) : 1657-1661, 1988
10) Fischetti VA : Streptococcal M protein ; molecular design and biological behavior. Clin Microbiol Rev **2** (3) : 285-300, 1989
11) Beall B, et al : Sequencing *emm*-specific PCR products for routine and accurate typing of group A streptococci. J Clin Microbiol **34** (4) : 953-958, 1996
12) Inagaki Y, et al : Serotyping of *Streptococcus pyogenes* isolated from common and severe invasive infections in Japan, 1990-5 ; implication of the T3 serotype strain-expansion in TSLS. Epidemiol Infect **119** (1) : 41-48, 1997
13) Ikebe T, et al : Changing prevalent T serotypes and *emm* genotypes of *Streptococcus pyogenes* isolates from streptococcal toxic shock-like syndrome (TSLS) patients in Japan. Epidemiol Infect **130** (3) : 569-572, 2003
14) Ikebe T, et al : Distribution of *emm* genotypes among group A *streptococcus* isolates from patients with severe invasive streptococcal infections in Japan, 2001-2005. Epidemiol Infect **135** (7) : 1227-1229, 2007
15) 清水方可 : 劇症型 A 群連鎖球菌感染症の病態と治療. 日本医事新報 **4081** : 92, 2002
16) Stevens DL, et al : Invasive group A streptococcal infection ; new concepts in antibiotic treatment. Int J Antimicrob Agent **4** (4) : 297-301, 1994
17) Burry W, et al : Intravenous immunogloburin therapy for toxic shock syndrome. JAMA **267** (24) : 3315-3316, 1992

沈思黙考 1

国境を考える

林　謙治　国立保健医療科学院院長

フランスの政治家はよく世界地図を広げ，それを眺めながら，グローバルの観点から政策づくりをするという話をどこかで読んだことがある．そのような立場ではないが，国際保健に関心を持つ一人として，世界地図を眺めながらあれやこれやと空想にふけるのが楽しみであり，時には思わぬ発見をすることもある．

アフリカの国々の国境線は一直線になっているところが多い．人間が心地よく居住するには，山，川，森，砂漠など，自然環境に沿って生活圏を築くのがエコロジーの原理にかなっている．ケニアとタンザニアの国境線は，ケニア側で言えばキスムという町の南部に当たるビクトリア湖畔から草原の上をまっしぐらに東南方向に走り，途中 5,896 mのキリマンジェロという山にぶつかるところを避けて，再び直線的にモンバサという町の南方のインド洋海岸にいたっている．距離にして 1,000 kmあまりある．

第二次世界大戦前では両国はひとまとまりとしてイギリスの植民地であった．それぞれ独立するときに，人が住んでいないステップ地帯を単純に線引きして国境とした．今でも遊牧するマサイ族や，牧草を求める動物が，雨期・乾期の交代時に民族大移動さながら自由に行き来している．

仮に国境を閉鎖したらどうなるだろうか？言わずとも知れず遊牧民や動物は全滅するであろう．陸続きの国境を持たない日本人には理解しにくいかもしれないが，人為的な境界は生態系を破壊しがちである．アフリカの開発が遅れる理由の一つは，人為的国境により産業が成立しうる圏域が分断されていると考えられなくもない．

直線国境は北米のアメリカ，カナダ，メキシコの間でも見られる．それどころかアメリカ国内の多くの州境がそうである．これも植民地の落とし子である．生態学的破壊を免れるには合衆国連邦を構築する以外方法がなかったかもしれない．

その点アジアの生活圏は自然環境により沿っているように思う．日本のような島国はそういう意味ではまことに幸運であった．占領されても海に囲まれているために，人為的な国境は引きにくかった．

江戸時代の藩は生活圏が比較的よく保たれていたと思う．廃藩置県によってできた東北のいくつかの県は，行政区分と生活圏が一致してないように見える．現在議論されている道州制の区分を考えるとき，生活圏を考慮していただきたい．

INFECTION AND IMMUNITY, Nov. 2009, p. 4806–4814 Vol. 77, No. 11
0019-9567/09/$12.00 doi:10.1128/IAI.00577-09

CD46 Transgenic Mouse Model of Necrotizing Fasciitis Caused by *Streptococcus pyogenes* Infection▽

Hidenori Matsui,[1]†* Yukie Sekiya,[1]† Masahiko Nakamura,[2]* Somay Yamagata Murayama,[1] Haruno Yoshida,[1] Tetsufumi Takahashi,[2] Ken'ichi Imanishi,[3] Kanji Tsuchimoto,[2] Takehiko Uchiyama,[3,4] Keisuke Sunakawa,[1] and Kimiko Ubukata[1]

Kitasato Institute for Life Sciences and Graduate School of Infection Control Sciences, Kitasato University, 5-9-1 Shirokane, Minato-ku, Tokyo 108-8641, Japan[1]; Center for Clinical Pharmacy and Clinical Sciences, School of Pharmaceutical Sciences, Kitasato University, 5-9-1 Shirokane, Minato-ku, Tokyo 108-8641, Japan[2]; Department of Microbiology and Immunology, Tokyo Women's Medical University School of Medicine, 8-1 Kawada-cho, Shinjuku-ku, Tokyo 162-8666, Japan[3]; and College of Human Science, Tokiwa University, 1-430-1 Miwa, Mito-shi, Ibaraki 310-8585, Japan[4]

Received 23 May 2009/Returned for modification 9 July 2009/Accepted 26 August 2009

We developed a human CD46-expressing transgenic (Tg) mouse model of subcutaneous (s.c.) infection into both hind footpads with clinically isolated 11 group A streptococcus (GAS) serotype M1 strains. When the severity levels of foot lesions at 72 h and the mortality rates by 336 h were compared after s.c. infection with 1×10^7 CFU of each GAS strain, the GAS472 strain, isolated from the blood of a patient suffering from streptococcal toxic shock syndrome (STSS), induced the highest severity levels and mortality rates. GAS472 led to a 100% mortality rate in CD46 Tg mice after only 168 h postinfection through the supervention of severe necrotizing fasciitis (NF) of the feet. In contrast, GAS472 led to a 10% mortality rate in non-Tg mice through the supervention of partial necrotizing cutaneous lesions of the feet. The footpad skin sections of CD46 Tg mice showed hemorrhaging and necrotic striated muscle layers in the dermis, along with the exfoliation of epidermis with intracellular edema until 48 h after s.c. infection with GAS472. Thereafter, the bacteria proliferated, reaching a 90-fold or 7-fold increase in the livers of CD46 Tg mice or non-Tg mice, respectively, for 24 h between 48 and 72 h after s.c. infection with GAS472. As a result, the infected CD46 Tg mice appeared to suffer severe liver injuries. These findings suggest that human CD46 enhanced the progression of NF in the feet and the exponential growth of bacteria in deep tissues, leading to death.

Group A streptococci (GAS), which are among the most common human pathogens, can cause a variety of uncomplicated superficial skin infections such as impetigo/pyoderma or throat infections, including streptococcal pharyngitis (sore throat) and tonsillitis (3). In addition, patients suffering from acute and complicated GAS infections, in particular streptococcal toxic shock syndrome (STSS) associated with severe necrotizing fasciitis (NF), have high mortality rates (4). M proteins, which attach to the cell wall, are one of the important virulence factors that GAS possess (15). The various GAS strains have more than 100 different antigenically distinguishable M proteins (46), and GAS serotype M1 strains are regarded as a highly virulent group (3).

Membrane cofactor protein (MCP; CD46), which is expressed in every cell type except erythrocytes, is implicated as a receptor for at least six human pathogens (four viruses and two bacteria), including measles virus (9, 31, 35), herpesvirus 6 (40), adenovirus groups B (17, 41) and D (48), pathogenic *Neisseria* (23), and GAS (37). Human CD46-expressing transgenic (Tg) mice are susceptible to streptococcal disease (30). When CD46 Tg and non-Tg mice were infected intravenously (i.v.) with GAS, the bacteremia levels, frequency of arthritis, and mortality rate were higher in CD46 Tg mice than in non-Tg mice (30). Unfortunately, this animal model does not reflect the natural infection process in the human host. Consequently, we have attempted to establish a CD46 Tg mouse model of skin and soft tissue infection with GAS that closely represents the human disease. If the disease pathogenesis in an animal model is in many ways very similar to that observed in humans, it will enable researchers to address a variety of questions regarding the development of urgently needed diagnostic methods and therapies. To the best of our knowledge, this is the first report to create the CD46 Tg mouse model of subcutaneous (s.c.) infection with GAS472 (a serotype M1 strain isolated from the blood of a patient suffering from STSS) into both hind footpads, thereby causing an acute disease that mimics severe NF in human.

MATERIALS AND METHODS

Bacterial strains and culture conditions. Beta-hemolytic GAS serotype M1 strains collected in Japan in 2006 are described in Table 1. GAS strains were preserved in 10% (wt/vol) skim milk and stored at −85°C until use. The frozen GAS strains were streaked onto sheep blood agar plates (Nippon Becton Dickinson, Tokyo, Japan) and cultured overnight at 37°C in a humidified 5% CO_2 incubator. Prior to their use in infection experiments, GAS strains were grown on Todd-Hewitt broth containing 0.2% (wt/vol) yeast extract (THY; Difco and BBL, Detroit, MI) in 5% CO_2 at 37°C without shaking.

* Corresponding author. Mailing address: Kitasato Institute for Life Sciences and Graduate School of Infection Control Sciences, Kitasato University, 5-9-1 Shirokane, Minato-ku, Tokyo 108-8641, Japan. Phone and fax for H. Matsui: 81-3-5791-6267. E-mail: hmatsui@lisci.kitasato-u.ac.jp. Phone and fax for M. Nakamura: 81-3-3446-9036. E-mail: nakamuram@pharm.kitasato-u.ac.jp.
† H.M. and Y.S. contributed equally.
▽ Published ahead of print on 8 September 2009.

TABLE 1. Characteristics of 11 clinical isolates of GAS serotype M1

GAS strain	Patient age (yr)	Patient sex	Diagnosis	Collection source	Patient survival status
GAS472	38	Male	STSS	Blood	Dead
GAS467	57	Male	Meningitis, sepsis	CSF[a]	Dead
RE335	6	Female	Pyogenic arthritis	Blood	Alive
RE025	76	Male	NF	Tissue specimens	Dead
GAS465	7	Female	Pharyngitis	Pharyngeal swab	Alive
RE386	62	Female	Pharyngitis, sinusitis	Blood	Alive
RE137	72	Male	Meningitis	CSF	Dead
RE303	52	Male	Sepsis[b]	SCA[c]	Dead
RE157	75	Male	Facial cellulitis	Blood	Alive
GAS453	9	Male	PCA[d]	Pharyngeal swab	Alive
RE344	40	Female	Sepsis[e]	Blood	Alive

[a] CSF, cerebrospinal fluid.
[b] Chronic renal failure (preexisting disease).
[c] SCA, subendocardial abscess.
[d] PCA, pyogenic cervical adenitis.
[e] Acute hepatitis (preexisting disease).

Mouse model for GAS infection. The human CD46-expressing Tg mice were a generous gift from J. P. Atkinson, Washington University. CD46 Tg mice possess two copies of human CD46 gene per diploid genome, and the expression levels of CD46 RNA and protein were comparable to those observed in matched human tissues, including muscle, fat, and skin (25). Using immunohistochemistry, human CD46 was found on epithelial cells, endothelial cells, glial cells, and hepatocytes; in the glomerulus (in kidney) and adrenal gland; as well as on B cells, T cells, neutrophils, and macrophages (22). The CD46 Tg mice used in this study had the C57BL/6 genetic background ($H\text{-}2^b$ haplotype). In previous studies, C57BL/6 (21, 22, 25, 34) or B6C3F1 ($H\text{-}2^{bk}$) (30, 42) mice have been used as non-Tg control mice. Therefore, to begin this study, we used both C57BL/6 and B6C3F1 mice obtained from Charles River Japan (Yokohama, Japan) as non-Tg control mice. The expression of many pathogenic traits of GAS has been shown to depend on the growth phase (33). Thus, 7-week-old mice were s.c. infected with a total of 1×10^7 CFU of stationary-growth-phase GAS into both hind footpads (5×10^6 CFU per footpad). After s.c. infection, the survival rates were observed every 24 h for 336 h postinfection, or the number of bacteria in the blood and tissue samples including the popliteal lymph nodes (PLN), spleen, and liver were determined by plating onto sheep blood agar (11, 27). All mice were bred at the animal facility at the Kitasato Institute, and all mouse experiments were performed in accordance with institutional protocol guidelines under an approved protocol.

Macroscopic and microscopic observations. Macroscopic images were obtained with a digital camera (D80; Nikon, Tokyo, Japan). For histological examination, a portion of each footpad and a portion of each liver were fixed with 10% (vol/vol) buffered formalin and then embedded in paraffin. Tissue sections approximately 5 μm thick were prepared and mounted on glass slides. The slides were stained with hematoxylin and eosin (H&E) and Giemsa. Alternatively, another portion of each liver was also fixed with Zamboni's fixative (2% [wt/vol] paraformaldehyde and 15% [vol/vol] saturated picric acid in 0.1 M phosphate buffer, pH 7.3) for at least 8 h at 4°C (44), and the 4-μm cryostat sections obtained were stained with Alexa Fluor 594-conjugated phalloidin (Molecular Probes, Eugene, OR) at a dilution of 1:1,000. The sections were mounted in Permafluor and were observed by confocal laser microscopy (TCS NT; Leica Biosystems, Nussloch, Germany).

Transcription analysis. The bacterial cells of GAS472 grown in THY broth were washed once with Dulbecco's modified Eagle's medium (Sigma-Aldrich, St. Louis, MO) and suspended in Dulbecco's modified Eagle's medium. The bacterial cell suspension (1×10^8 CFU) was mixed with an equal volume of whole blood from CD46 Tg or C57BL/6 mice collected by cardiac puncture with a heparin-coated 23-gauge needle. The mixture was then placed in a 37°C humidified 5% CO_2 incubator. At 0, 1, 2, and 6 h of incubation, bacterial cells were harvested by centrifugation and washed three times with cold distilled water. Gene expression patterns of GAS472 were determined by quantitative real-time reverse transcription (RT)-PCR analysis. Total RNA extracted from bacterial cells using the RNeasy Protect bacteria minikit with on-column RNase-free DNase I treatment (Qiagen Sciences, Germantown, MD) was subjected to the RT reaction from 100 ng of total RNA in a 20-μl reaction volume using the iScript cDNA synthesis kit (Bio-Rad Laboratories, Hercules, CA). The following real-time PCR assays were performed with RNA templates to ensure that contaminating genomic DNA was absent before the RT reaction. Quantitative real-time PCR in triplicate on 1 μl of template cDNA per 10-μl reaction was performed in a CFX96 real-time PCR detection system (Bio-Rad Laboratories) using the iQ SYBR green supermix (Bio-Rad Laboratories). Gene-specific primer pairs (16S rRNA, 5′-GAGAGACTAACGCATGTTAGTA-3′ and 5′-TAGTTACCGTCACTTGGTGG-3′; *sagA*, 5′-TGCTGCTGCTGCTGTACTAC-3′ and 5′-GCTTCCGCTACCACCTTGAG-3′) were designed using Beacon Designer 7.5. The PCR conditions included an initial denaturation step at 95°C for 3 min, followed by 50 amplification cycles of denaturation at 95°C for 10 s, annealing at 52°C for 10 s, and extension at 72°C for 30 s.

Genotypic analysis of GAS. For a comparison of the DNA sequences of the *csrRS* (also called *covRS*) locus between virulent (GAS472 and GAS467) and avirulent (RE386 and RE344) strains of GAS, we used 12 primers (p1 to p12) as previously described by Walker et al. (47). We used an ABI 3130 automatic sequencer (Applied Biosystems, Foster City, CA) for the direct sequence of the amplified PCR products (3,018 bp) with the primer pair p1/p12. The determined DNA sequences were assembled by the use of a component of Vector NTI version10.3.1 (Invitrogen, Carlsbad, CA).

Statistics. Significant differences between the means ± standard deviations (SDs) of different groups were examined using a two-tailed unpaired Student's *t* test (see Fig. 6) or a one-tailed paired Student's *t* test (see Fig. 8). A P value of <0.05 was regarded as statistically significant.

RESULTS

CD46 Tg mice exhibited necrotizing lesions of the feet 72 h after s.c. infection with GAS strains. As shown in Fig. 1, we classified 11 GAS strains into two groups associated with the severity levels of foot lesions in CD46 Tg mice 72 h after infection with GAS strains. In the first group, the feet developed well-defined necrosis (GAS472, GAS467, and RE025). The second group showed swelled feet (the skin appeared red and blotchy) and occasionally blisters (RE335, GAS465, GAS453, RE303, RE386, RE137, RE157, and RE344). All infected CD46 Tg mice were still alive in this time period. In contrast, even in the worst cases, the necrotizing cutaneous lesions developed partially in the feet of non-Tg mice 72 h after infection with GAS472 (Fig. 2A and B). Alternatively, the feet merely swelled up or developed minor wounds in non-Tg mice 72 h after infection with GAS467 (Fig. 2C and D) or RE335 (Fig. 2E and F). These results demonstrate that GAS472 had the strongest virulence traits among the 11 GAS strains essential for causing necrotizing lesions. Accordingly, we selected and used GAS472 for the following histological study.

The footpad skin sections of CD46 Tg and non-Tg mice

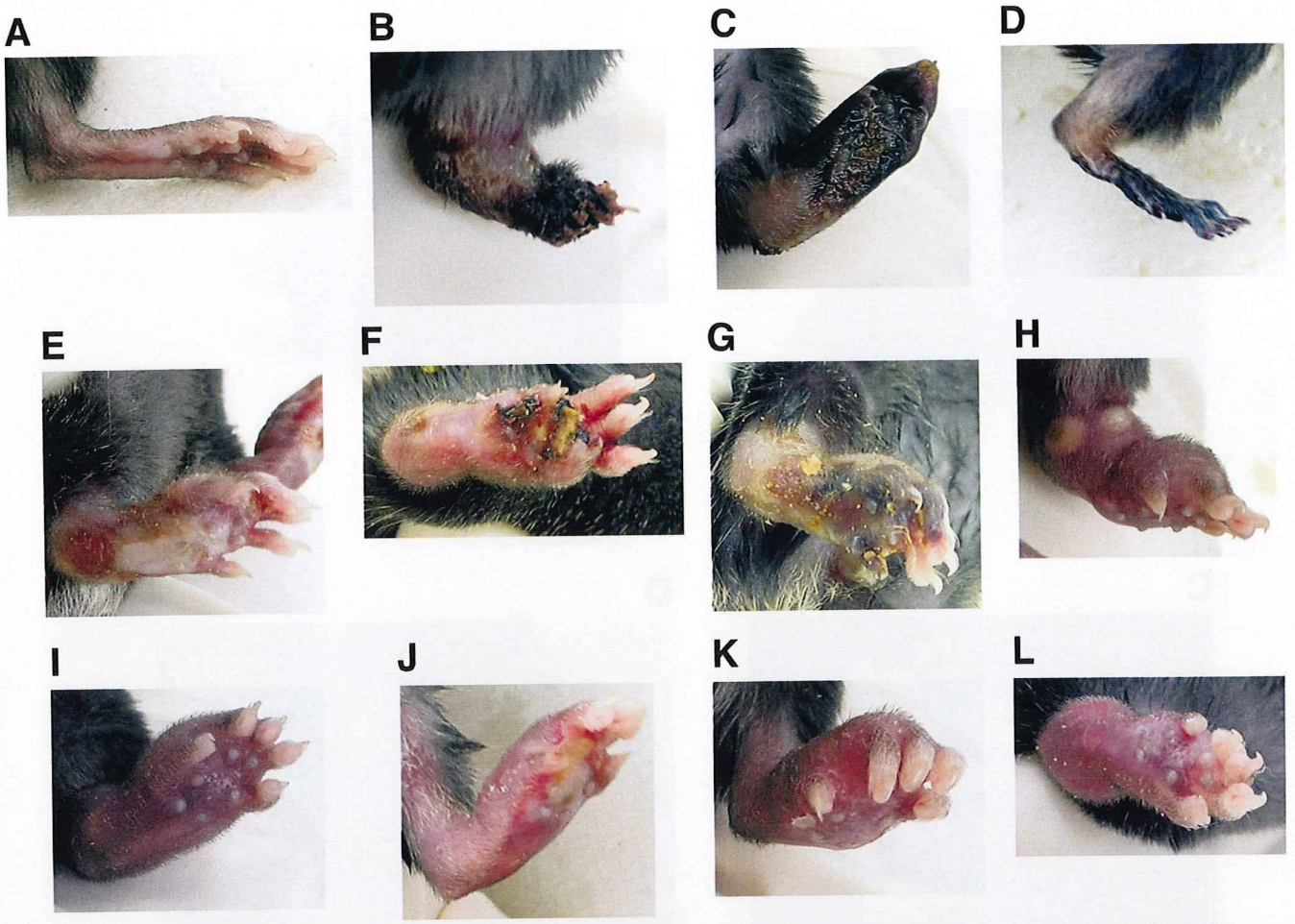

FIG. 1. Representative appearance of necrotizing lesions of CD46 Tg mouse feet. Shown is the macroscopic observation of CD46 Tg mouse foot 72 h after s.c. infection with 5×10^6 CFU of the GAS strains GAS472 (B), GAS467 (C), RE025 (D), RE335 (E), GAS465 (F), GAS453 (G), RE303 (H), RE386 (I), RE137 (J), RE157 (K), and RE344 (L) per footpad. Panel A shows noninfection.

exhibited acute inflammation (neutrophil infiltration) in the hypodermis 6 h after infection with GAS472. At 24 h postinfection, although increased inflammatory cell infiltration was recognized in the dermis of CD46 Tg and non-Tg mice, higher numbers of inflammatory cells were observed in the non-Tg mice (Fig. 3B and E). In addition, exfoliation of epidermis with intracellular edema and hemorrhaging in the dermis developed in CD46 Tg mice (Fig. 3B). At 48 h postinfection, the necrotic striated muscle layers were recognized in the dermis of CD46 Tg mice (Fig. 3C). In contrast, although the exfoliation of epidermis was observed, the necrosis could not yet be detected in the dermis of non-Tg mice at this stage (Fig. 3F).

These findings suggest that s.c. infection with GAS472 rapidly led to severe NF in the feet of CD46 Tg mice.

s.c. infection with GAS472 had a 100% mortality rate in CD46 Tg mice. As shown in Fig. 4, we observed differences in susceptibility of CD46 Tg mice after infection with 11 GAS strains. As a result, the mortality rates of the 336-h observation period were ranked in the following order: GAS472 (100%) > RE335 (83%) > GAS467 (67%) > RE025 (50%) > RE157 = GAS453 (43%) > GAS465 = RE137 (29%) > RE303 = RE386 = RE344 (0%). Therefore, we chose GAS472, RE335, and GAS467 as the three most virulent of the 11 GAS strains concerning the susceptibility of CD46 Tg mice. We then newly infected CD46 Tg and non-Tg mice with GAS472, RE335, or GAS467 at the same time. As shown in Fig. 5, the mortality rates among non-Tg mice were extremely low (0 or 10%). The differences in mortality rates between C57BL/6 and B6C3F1 mice after infection with each GAS strain were almost negligible. Thus, GAS472 was regarded as the most virulent strain in terms of the progression of NF and the susceptibility of CD46 Tg mice among 11 GAS strains.

s.c. infection with GAS472 was associated with a high level of bacterial load in deep tissues of CD46 Tg mice. As shown in Fig. 6, CD46 Tg mice had a significantly higher number of viable bacteria in each blood, spleen, and liver sample compared with non-Tg mice 48 h after infection with GAS472. Thereafter, the viable bacterial numbers in the blood and in every tissue sample increased 72 h after infection in CD46 Tg mice. Especially, the number of bacteria increased 90-fold in the livers of CD46 Tg mice for 24 h from 48 h to 72 h postinfection. In contrast, the number of bacteria increased sevenfold in the livers of non-Tg mice for 24 h from 48 h to 72 h postinfection. In other words, the estimated bacterial doubling

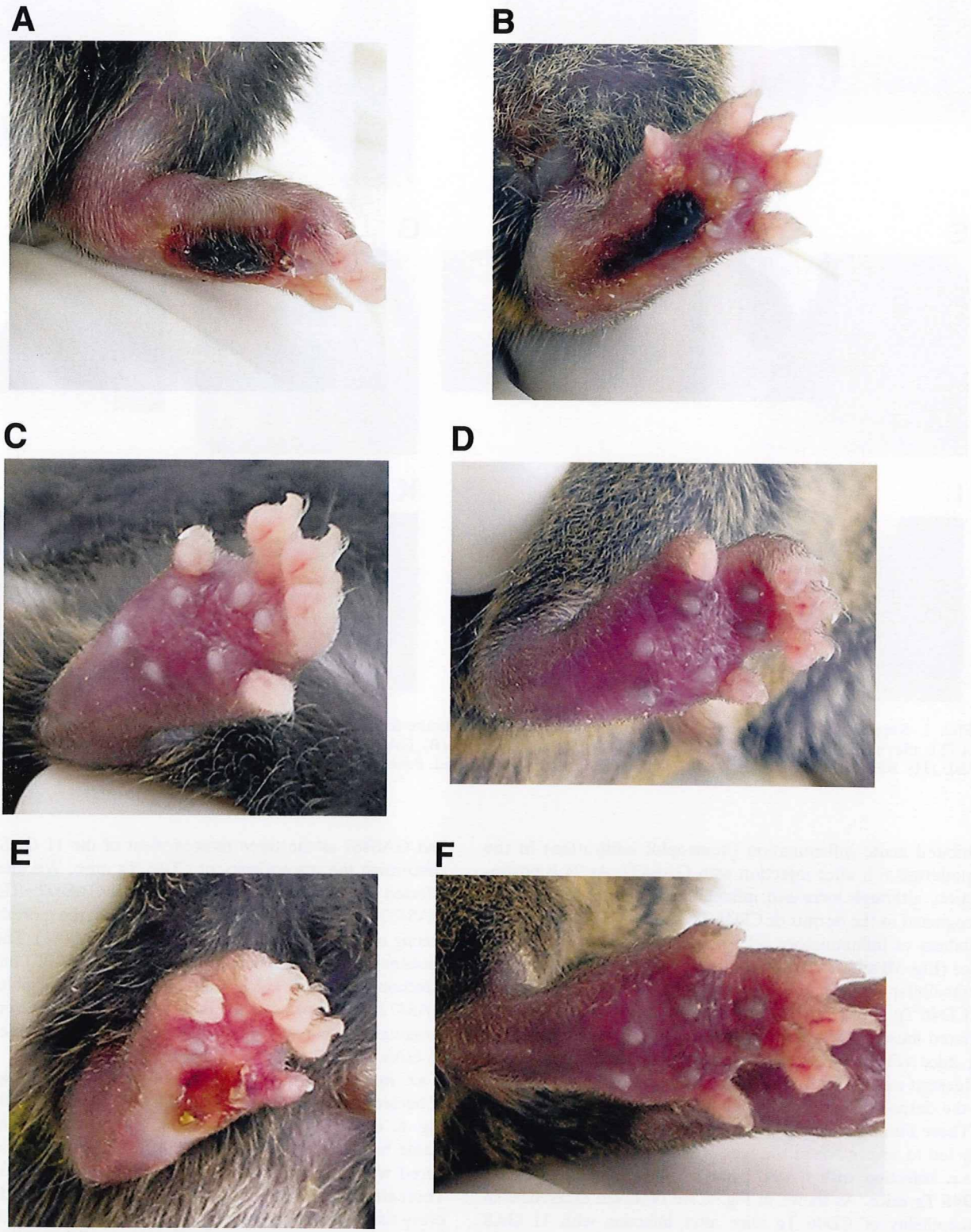

FIG. 2. Representative appearance of mild cutaneous lesions of non-Tg mouse feet. Shown is the macroscopic observation of C57BL/6 (A, C, and E) or B6C3F1 (B, D, and F) mouse foot 72 h after s.c. infection with 5×10^6 CFU of GAS strain GAS472 (A and B), GAS467 (C and D), or RE335 (E and F) per footpad.

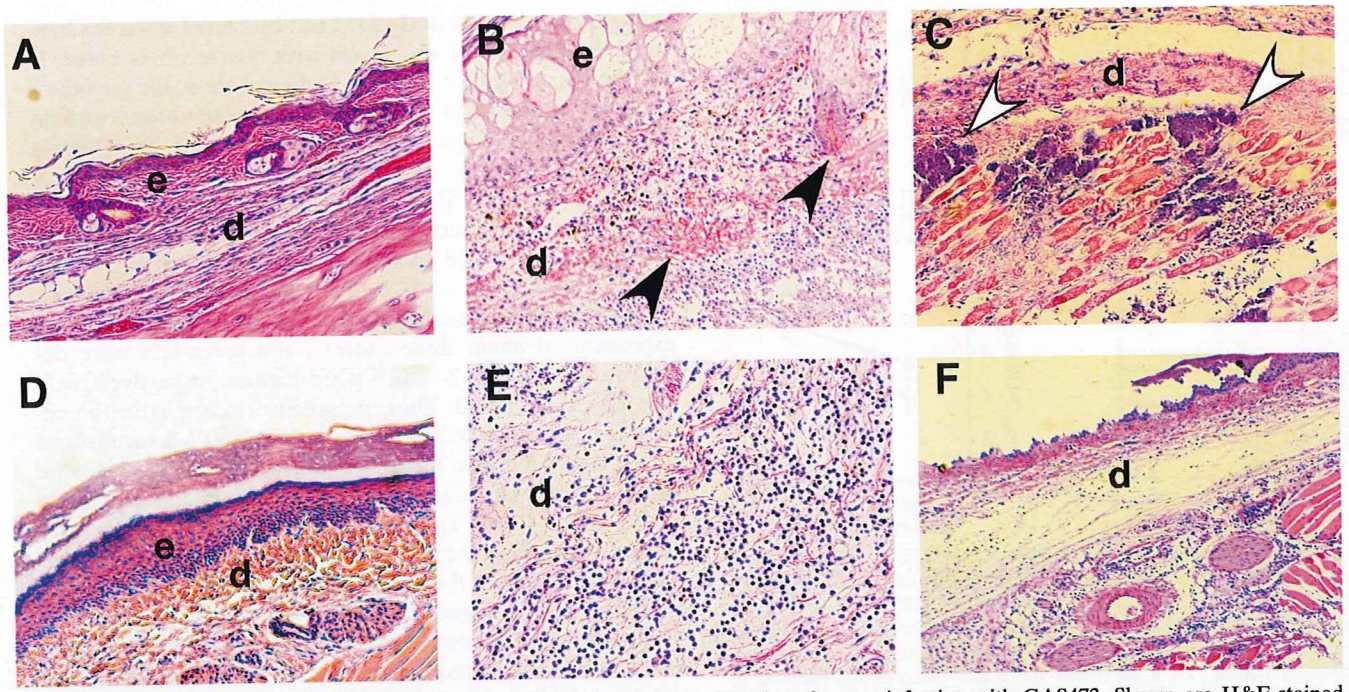

FIG. 3. Histological observation of footpad skin of CD46 Tg and non-Tg mice after s.c. infection with GAS472. Shown are H&E-stained footpad skin sections from CD46 Tg (A to C) and C57BL/6 (D to F) mice after s.c. infection with 5×10^6 CFU of GAS472 per footpad. (A and D) Uninfected. Original magnification, × 100. (B and E) Twenty-four hours after infection. Original magnification, ×200. (C and F) Forty-eight hours after infection. Original magnification, ×100. The closed arrowheads indicate hemorrhaging in the dermis. The open arrowheads indicate the necrotic striated muscle layers. e, epidermis; d, dermis.

times during these 24 h were 3.7 h and 8.5 h in the livers of CD46 Tg and non-Tg mice, respectively.

s.c. infection with GAS472 induced hepatic damage in CD46 Tg mice. Macroscopic observations showed the development of granulomatous nodules in the CD46 Tg mouse liver 72 h after s.c. infection with GAS472 (Fig. 7A). Simultaneously, microscopic observations revealed the development of full porous cytoplasmic F-actin bundles (Fig. 7C) in the liver sections of CD46 Tg mice after infection. Multifocal areas of necrosis were associated with inflammatory infiltrate (Fig. 7D), and clusters of streptococci were visible at the edges of the necrotic areas (Fig. 7E) in the liver sections of CD46 Tg mice after infection. Based on these results, we considered it likely that s.c. infection with GAS472 induced hepatic damage in CD46 Tg mice along with NF in their feet.

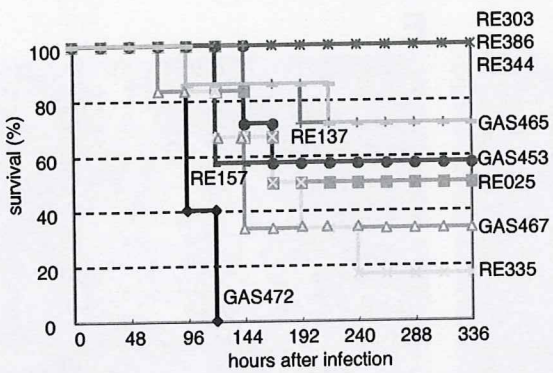

FIG. 4. Comparison of survival curves of CD46 Tg mice after s.c. infection with GAS strains. The mice infected s.c. with 5×10^6 CFU of GAS strains per footpad were monitored every 24 h for survival during the 336-h study. $n = 7$ for GAS453, RE137, RE157, and GAS465; $n = 6$ for RE335, GAS467, RE025, RE303, RE344, and RE386; and $n = 5$ for GAS472.

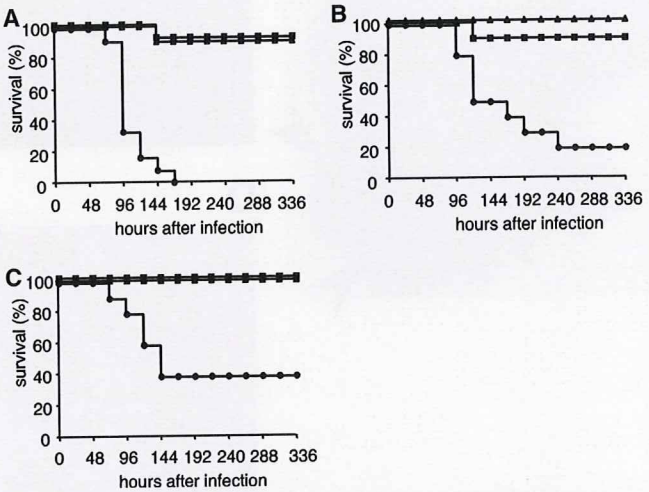

FIG. 5. Comparison of survival rates between CD46 Tg and non-Tg mice after s.c. infection with GAS strains. CD46 Tg and non-Tg (C57BL/6 and B6C3F1) mice were infected s.c. with 5×10^6 CFU of GAS472 (A), RE335 (B), or GAS467 (C) per footpad. The mice were then monitored every 24 h for survival during the 336-h study. Closed circles, CD46 Tg mice (A, $n = 12$; B and C, $n = 10$); closed squares, C57BL/6 mice (A, $n = 12$; B and C, $n = 10$); closed triangles, B6C3F1 mice (A and C, $n = 11$; B, $n = 10$).

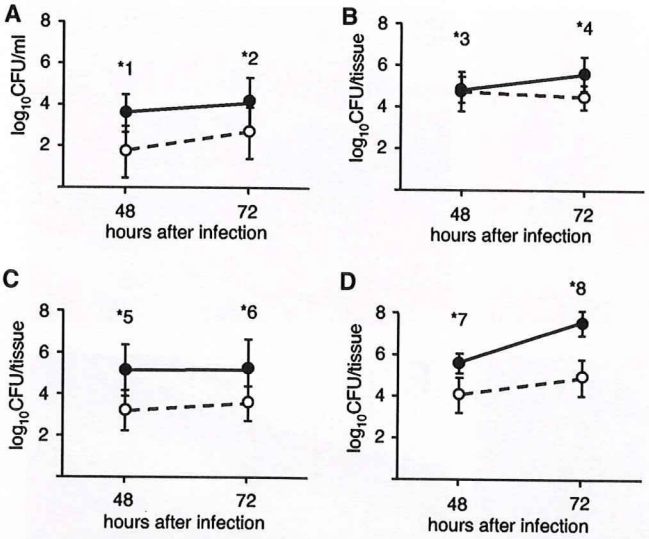

FIG. 6. Comparison of growth rates of GAS472 in the blood, PLN, spleen, and liver of mice. CD46 Tg (closed circles) and C57BL/6 (open circles) mice were infected s.c. with 5×10^6 CFU of GAS472 per footpad. At 48 and 72 h postinfection, the numbers of bacteria in the blood (A), PLN (B), spleen (C), and liver (D) samples were determined by plating. Data represent the mean value of the number of bacteria per ml (blood) or per tissue sample (PLN, spleen, and liver) ± SD. *1, $P = 0.001$; *2, $P = 0.02$; *3, $P = 0.77$; *4, $P = 0.002$; *5, $P = 0.001$; *6, $P = 0.008$; *7, $P = 0.00009$; *8, $P = 0.0000003$ (CD46 Tg mice versus non-Tg mice; $n = 10$).

Expression of *sagA* in GAS472 was increased when the bacterial cell suspension was mixed with mouse whole blood. It was demonstrated that during 6 h of incubation, the growth of GAS was enhanced in the cell culture medium mixed with an equal volume of mouse whole blood containing soluble human CD46 (30). Then, we examined the changes in expression of *sagA* (streptolysin S; SLS) of GAS472 during 6 h of incubation under the above experimental conditions. As shown in Fig. 8, ~3-, 30-, and 30-fold increases in expression of *sagA* were detected during the 1-, 2-, and 6-h incubations, respectively, with CD46 Tg mouse blood. In contrast, *sagA* increases in expression of about three-, seven-, and seven-fold were detected during the 1-, 2-, and 6-h incubations, respectively, with non-Tg mouse blood. Thus, progressive increases in the expression of *sagA* detected during the 2-h and 6-h incubations were CD46 Tg mouse blood dependent. The differences were not significant (P values of >0.05), although the expression levels of the CD46 Tg mouse blood-dependent group were higher than those of the non-Tg mouse blood-dependent group in all three of the experiments. Although we also examined for changes in gene expression of *emm* (M protein), *csrS* (sensor histidine kinase), *scpA* (C5a peptidase), *scpC* (serine protease), *ska* (streptokinase), *speB* (cystein protease), and *speA* (streptococcal pyrogenic exotoxin A) using real-time RT-PCR with each gene-specific primer pair, significant changes in gene expression were not detected during the 6-h incubation with CD46 Tg or non-Tg mouse blood.

In the meantime, it was also demonstrated that CsrRS (a

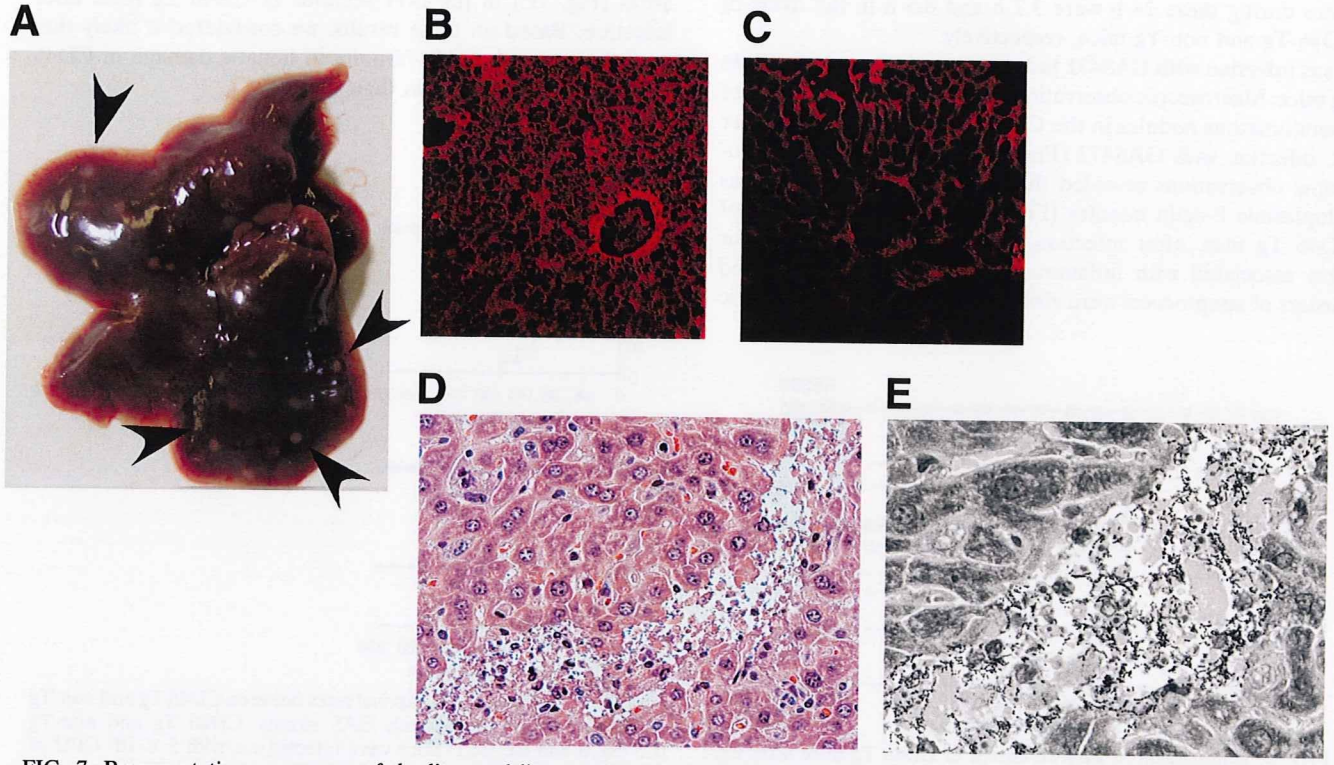

FIG. 7. Representative appearance of the liver and liver sections of CD46 Tg mice. Shown are a macroscopic observation of liver (A), a fluorescent phalloidin F-actin staining image (red) of a liver section (C), an H&E-stained liver section (D), and a Giemsa-stained liver section (E) of a CD46 Tg mouse 72 h after s.c. infection with 5×10^6 CFU of GAS472 per footpad. The immunofluorescence image of a liver section from an uninfected CD46 Tg mouse (B) is also shown. B, C, D, and E, original magnifications ×100, ×100, ×200, and ×400, respectively. The arrowheads indicate the granulomatous nodules in the liver.

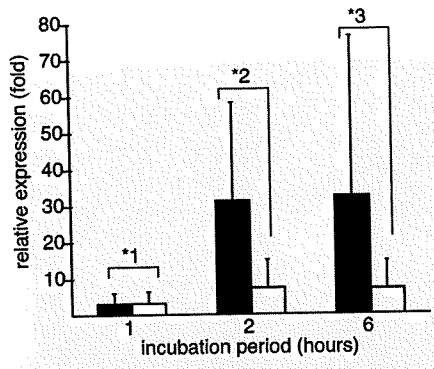

FIG. 8. Gene expression profile of GAS472 during the incubation period. Total RNA was prepared from bacterial cells, and quantitative real-time RT-PCR was carried out as described in Materials and Methods. At each time point, the expressional level of *sagA* was normalized to the corresponding 16S rRNA gene value. In addition, each normalized value was then converted to reflect the amplification of each value for zero time. Data represent the mean values ± SDs of three independent experiments. Closed columns, bacterial cell suspension with CD46 Tg mouse blood; open columns, bacterial cell suspension with C57BL/6 mouse blood. *1, $P = 0.25$; *2, $P = 0.08$; *3, $P = 0.17$ (CD46 Tg mouse blood versus non-Tg mouse blood).

member of the two-component regulatory system) influenced the transcription of 15% of all chromosomal genes of GAS, including negative controls on the gene expression of five virulence factors (capsule, cystein protease, streptokinase, SLS, and streptodornase) (18). Since recent studies showed that the mutation of *csrRS* was important for the invasive phenotype of GAS (2, 45), we compared the DNA sequences of *csrRS* among two virulent strains (GAS472 and GAS467), two avirulent strains (RE386 and RE344), and a type strain of GAS serotype M1 (MGAS5005). No DNA sequence variations were identified inside the coding regions of *csrRS* among GAS472 (accession no. AB513958), GAS467 (accession no. AB513957), RE386 (accession no. AB513956), RE344 (accession no. AB513955), and MGAS5005 (accession no. NC_007297). Instead, the following two variations were found in the 5′ noncoding regions of *csrRS*: variation 1, c.−55_−56insT (a single nucleotide insertion of T in GAS472, GAS467, RE386, and RE344 at the position between −55 and −56 from the TTG initiation codon of *csrS* in MGAS5005); and variation 2, c.−232delA (a single nucleotide deletion of A in GAS472 at position −232 from the ATG initiation codon of *csrR* in MGAS5005).

DISCUSSION

In human patients, NF due to GAS infection is defined pathologically by a deep-seated infection of the s.c. tissue that results in the progressive destruction of fascia and fat, with relative sparing of skeletal muscle (4, 13, 16, 28). NF is rare in young children but more common in otherwise healthy adults, in whom a minor skin wound often precedes the disease, as was reported in a case study of a 25-year-old man (13). That study showed extensive bands of liquefactive necrosis and patchy inflammation of the deep dermis and subcutis in specimens of the patient's skin and soft tissue (13). Moreover, a focal abscess with numerous degenerating neutrophils formed in the deep dermis in that case (13). These symptoms closely resemble the skin specimens of CD46 Tg mice after s.c. infection with GAS472, as described in Fig. 3.

In previously published mouse models of skin and soft tissue infection with GAS, the bacteria were inoculated s.c. into the backs (8, 32, 36), haunches (6), or flanks (1, 5, 7, 38). Compared to such models, the s.c. inoculation into both hind footpads in the present study was a simple procedure, and the obtained data showed a narrow dispersion of reproducibility. A recent study demonstrated that infection in epithelial cells with GAS led to the shedding of human CD46 at the same time as bacterium-induced apoptosis and cell death occurred (30). In the present study, the amount of bacterial load in the PLN of CD46 Tg mice was the same as that of non-Tg mice 48 h after s.c. infection (Fig. 6B), indicating that the same amounts of bacteria resided in the feet of CD46 Tg and non-Tg mice for 48 h after s.c. infection. However, since the progression of NF until 48 h after s.c. infection was dramatically elevated in the feet of CD46 Tg mice compared to those of non-Tg mice (Fig. 3), human CD46-mediated GAS infection was thought to be necessary for the observed acceleration of disease progression in the mouse feet. Interestingly, in many cases, non-Tg mouse feet were completely extinguished by persistent necrosis of skin, soft tissue, and bone up to 336 h after infection with GAS472, although the mice were still alive (Fig. 9A). In addition, the majority of CD46 Tg mouse feet were also lost by persistent necrosis no later than 336 h after infection with even avirulent GAS strains other than GAS472, GAS467, and RE025 (Fig. 9B). Possibly, such persistent necrosis due to GAS infection cannot lead to death in CD46 Tg and non-Tg mice.

We classified 11 clinical isolates into the virulent or avirulent strains of GAS based on the severity levels of foot lesions at 72 h and the mortality rates by 336 h after s.c. infection. RE303 and RE344 did not show the capacity to induce lethal disease in CD46 Tg mice (Fig. 4), despite the fact that they were recovered from patients with invasive diseases (Table 1). In both cases, the patients were immunocompromised due to preexisting diseases. Supposedly, even avirulent GAS strains are able to induce invasive diseases in the patients suffering from preexisting medical conditions.

According to a previous report, GAS infection was commonly associated with the early onset of shock and organ failure in humans (4). Another recent study demonstrated that GAS might bind available extracellular CD46 as a strategy to survive and avoid host defenses and that the lethal disease and arthritis were much more frequent in CD46 Tg mice than in non-Tg mice after i.v. infection with GAS (30). Our data clearly indicate that the proliferation rate during the 24 h between 48 and 72 h after s.c. infection with GAS472 in the liver was much higher in CD46 Tg mice than in non-Tg mice (Fig. 6D). Indeed, bacterial infection induced serious liver damage in CD46 Tg mice (Fig. 7). Probably, human CD46 potentially ensures bacterial growth in the deep tissues. Thereafter, systemic GAS infection might lead to organ failure and ultimately to the death of the mice.

The M proteins appear as long, hairlike filaments on the bacterial surface and are composed of two α-helical chains that are predominantly arranged in a coiled-coil conformation (14). All of the M proteins contain a conserved C-terminal region near the cell surface and a hypervariable N-terminal region

FIG. 9. Ultimate appearance of the mouse feet. Shown is a macroscopic observation of a C57BL/6 (A) or CD46 Tg (B) mouse foot 336 h after s.c. infection with 5×10^6 CFU of GAS472 or RE137 per footpad, respectively.

that provides the basis for serological typing (14). A function of M proteins was shown to be critical for protecting organisms from phagocytosis (14). An in vitro invasion study using A549 human lung epithelial cells demonstrated that the M protein-promoted ingestion of GAS was dependent on the coengagement of CD46 and α5β1 integrin (39). In addition, CD46-mediated invasion was also found to depend on the extracellular matrix protein fibronectin (39). CD46 has been generally recognized as a regulator of the complement system that facilitates factor I-mediated inactivation of the activated complement proteins C3b and C4b (29). In the meanwhile, the interaction between GAS and CD46 triggered cell signaling pathways that directly induced an immunosuppressive phenotype in T cells (26). In fact, by immunohistochemistry, M protein/fibrinogen complexes were identified in tissue biopsies from a patient suffering from NF and STSS (19). Recently, it was shown that the binding of CD46 to GAS serotype M18 strains was independent of Emm (M protein) or Enn (immunoglobulin A-binding protein) (12). There may be some biological advantages to GAS having Emm-dependent and Emm-independent CD46-binding abilities. In any case, whether or not the M1 protein directly responded to human CD46 in the host cell, we suppose that the human CD46-dependent regulation of virulence gene expression in GAS serotype M1 strains should be necessary for the induction of both local inflammation and deep tissue damage in the CD46 Tg mouse model.

It is well known that ScpC can cleave interleukin-8, a chemokine that mediates neutrophil transmission and activation (10, 20). The ScpC mutant strain did not degrade interleukin-8 and thus failed to prevent recruitment of immune cells; also, it caused disease after soft tissue infection (43), whereas the increased expression of ScpC and streptolysin O (a membrane-damaging extracellular toxin) caused by *csrS* mutation played a prominent role in the mouse model of GAS infection (2). Meanwhile, since GAS serotype M1 strains isolated from invasive diseases in human had mutation accumulation at the *csrRS* locus, resulting in an SpeB-negative phenotype (45), the SpeB expression levels of GAS serotype M1 strains were thought to be inversely correlated with disease severity in humans (24). In fact, an SpeB-negative phenotype caused by the *csrRS* mutation was a more virulent strain of GAS than the wild-type strain in the mouse model (47). Consequently, we had expected that GAS472 gained any mutation inside the coding regions of *csrRS* during infection, resulting in the high-virulence phenotype. Against our expectation, no DNA sequence variation was found inside the coding regions of *csrRS* in virulent strains (GAS472 and GAS467) or avirulent strains (RE344 and RE386) compared to a standard strain (MGAS5005). Unexpectedly, however, it became clear that the high-virulence phenotypes were not due to the mutation of *csrRS*. Therefore, the most significant questions—regarding genetic differences and virulence genes in different strains and how the virulent strains cause serious and lethal disease in humans—remain unanswered.

ACKNOWLEDGMENTS

We are grateful to John P. Atkinson for kindly providing the CD46 Tg mouse strain.

This work was financially supported by a grant under the category "Research Projects for Emerging and Re-emerging Infectious Diseases" (H-19-002 and H-20-002) from the Ministry of Health, Labor and Welfare of Japan.

We declare that no conflict of interest exists.

REFERENCES

1. **Ashbaugh, C. D., H. B. Warren, V. J. Carey, and M. R. Wessels.** 1998. Molecular analysis of the role of the group A streptococcal cysteine protease, hyaluronic acid capsule, and M protein in a murine model of human invasive soft-tissue infection. J. Clin. Investig. **102**:550–560.
2. **Ato, M., T. Ikebe, H. Kawabata, T. Takemori, and H. Watanabe.** 2008. Incompetence of neutrophils to invasive group A streptococcus is attributed to induction of plural virulence factors by dysfunction of a regulator. PLoS ONE **3**:e3455.
3. **Aziz, R. K., and M. Kotb.** 2008. Rise and persistence of global M1T1 clone of *Streptococcus pyogenes*. Emerg. Infect. Dis. **14**:1511–1517.
4. **Bisno, A. L., and D. L. Stevens.** 1996. Streptococcal infections of skin and soft tissues. N. Engl. J. Med. **334**:240–245.
5. **Brenot, A., K. Y. King, B. Janowiak, O. Griffith, and M. G. Caparon.** 2004.

Contribution of glutathione peroxidase to the virulence of *Streptococcus pyogenes*. Infect. Immun. **72**:408–413.
6. **Dalton, T. L., R. I. Hobb, and J. R. Scott.** 2006. Analysis of the role of CovR and CovS in the dissemination of *Streptococcus pyogenes* in invasive skin disease. Microb. Pathog. **40**:221–227.
7. **Datta, V., S. M. Myskowski, L. A. Kwinn, D. N. Chiem, N. Varki, R. G. Kansal, M. Kotb, and V. Nizet.** 2005. Mutational analysis of the group A streptococcal operon encoding streptolysin S and its virulence role in invasive infection. Mol. Microbiol. **56**:681–695.
8. **Di Nardo, A., K. Yamasaki, R. A. Dorschner, Y. Lai, and R. L. Gallo.** 2008. Mast cell cathelicidin antimicrobial peptide prevents invasive group A *Streptococcus* infection of the skin. J. Immunol. **180**:7565–7573.
9. **Dorig, R. E., A. Marcil, A. Chopra, and C. D. Richardson.** 1993. The human CD46 molecule is a receptor for measles virus (Edmonston strain). Cell **75**:295–305.
10. **Edwards, R. J., G. W. Taylor, M. Ferguson, S. Murray, N. Rendell, A. Wrigley, Z. Bai, J. Boyle, S. J. Finney, A. Jones, H. H. Russell, C. Turner, J. Cohen, L. Faulkner, and S. Sriskandan.** 2005. Specific C-terminal cleavage and inactivation of interleukin-8 by invasive disease isolates of *Streptococcus pyogenes*. J. Infect. Dis. **192**:783–790.
11. **Eguchi, M., Y. Sekiya, M. Suzuki, T. Yamamoto, and H. Matsui.** 2007. An oral *Salmonella* vaccine promotes the down-regulation of cell surface Toll-like receptor 4 (TLR4) and TLR2 expression in mice. FEMS Immunol. Med. Microbiol. **50**:300–308.
12. **Feito, M. J., A. Sanchez, M. A. Oliver, D. Perez-Caballero, S. Rodriguez de Cordoba, S. Alberti, and J. M. Rojo.** 2007. Membrane cofactor protein (MCP, CD46) binding to clinical isolates of *Streptococcus pyogenes*: binding to M type 18 strains is independent of Emm or Enn proteins. Mol. Immunol. **44**:3571–3579.
13. **Filbin, M. R., D. C. Ring, M. R. Wessels, L. L. Avery, and R. L. Kradin.** 2009. Case records of the Massachusetts General Hospital. Case 2-2009. A 25-year-old man with pain and swelling of the right hand and hypotension. N. Engl. J. Med. **360**:281–290.
14. **Fischetti, V. A.** 1989. Streptococcal M protein: molecular design and biological behavior. Clin. Microbiol. Rev. **2**:285–314.
15. **Fischetti, V. A., K. F. Jones, S. K. Hollingshead, and J. R. Scott.** 1988. Structure, function, and genetics of streptococcal M protein. Rev. Infect. Dis. **10**(Suppl. 2):S356–S359.
16. **Fustes-Morales, A., P. Gutierrez-Castrellon, C. Duran-Mckinster, L. Orozco-Covarrubias, L. Tamayo-Sanchez, and R. Ruiz-Maldonado.** 2002. Necrotizing fasciitis: report of 39 pediatric cases. Arch. Dermatol. **138**:893–899.
17. **Gaggar, A., D. M. Shayakhmetov, and A. Lieber.** 2003. CD46 is a cellular receptor for group B adenoviruses. Nat. Med. **9**:1408–1412.
18. **Graham, M. R., L. M. Smoot, C. A. Migliaccio, K. Virtaneva, D. E. Sturdevant, S. F. Porcella, M. J. Federle, G. J. Adams, J. R. Scott, and J. M. Musser.** 2002. Virulence control in group A *Streptococcus* by a two-component gene regulatory system: global expression profiling and in vivo infection modeling. Proc. Natl. Acad. Sci. USA **99**:13855–13860.
19. **Herwald, H., H. Cramer, M. Morgelin, W. Russell, U. Sollenberg, A. Norrby-Teglund, H. Flodgaard, L. Lindbom, and L. Bjorck.** 2004. M protein, a classical bacterial virulence determinant, forms complexes with fibrinogen that induce vascular leakage. Cell **116**:367–379.
20. **Hidalgo-Grass, C., M. Dan-Goor, A. Maly, Y. Eran, L. A. Kwinn, V. Nizet, M. Ravins, J. Jaffe, A. Peyser, A. E. Moses, and E. Hanski.** 2004. Effect of a bacterial pheromone peptide on host chemokine degradation in group A streptococcal necrotising soft-tissue infections. Lancet **363**:696–703.
21. **Johansson, L., A. Rytkonen, P. Bergman, B. Albiger, H. Kallstrom, T. Hokfelt, B. Agerberth, R. Cattaneo, and A. B. Jonsson.** 2003. CD46 in meningococcal disease. Science **301**:373–375.
22. **Johansson, L., A. Rytkonen, H. Wan, P. Bergman, L. Plant, B. Agerberth, T. Hokfelt, and A. B. Jonsson.** 2005. Human-like immune responses in CD46 transgenic mice. J. Immunol. **175**:433–440.
23. **Kallstrom, H., M. K. Liszewski, J. P. Atkinson, and A. B. Jonsson.** 1997. Membrane cofactor protein (MCP or CD46) is a cellular pilus receptor for pathogenic *Neisseria*. Mol. Microbiol. **25**:639–647.
24. **Kansal, R. G., A. McGeer, D. E. Low, A. Norrby-Teglund, and M. Kotb.** 2000. Inverse relation between disease severity and expression of the streptococcal cysteine protease, SpeB, among clonal M1T1 isolates recovered from invasive group A streptococcal infection cases. Infect. Immun. **68**:6362–6369.
25. **Kemper, C., M. Leung, C. B. Stephensen, C. A. Pinkert, M. K. Liszewski, R. Cattaneo, and J. P. Atkinson.** 2001. Membrane cofactor protein (MCP; CD46) expression in transgenic mice. Clin. Exp. Immunol. **124**:180–189.
26. **Kemper, C., J. W. Verbsky, J. D. Price, and J. P. Atkinson.** 2005. T-cell stimulation and regulation: with complements from CD46. Immunol. Res. **32**:31–43.
27. **Kodama, C., M. Eguchi, Y. Sekiya, T. Yamamoto, Y. Kikuchi, and H. Matsui.** 2005. Evaluation of the Lon-deficient *Salmonella* strain as an oral vaccine candidate. Microbiol. Immunol. **49**:1035–1045.
28. **Leitch, H. A., A. Palepu, and C. M. Fernandes.** 2000. Necrotizing fasciitis secondary to group A streptococcus. Morbidity and mortality still high. Can. Fam. Physician **46**:1460–1466.
29. **Liszewski, M. K., T. W. Post, and J. P. Atkinson.** 1991. Membrane cofactor protein (MCP or CD46): newest member of the regulators of complement activation gene cluster. Annu. Rev. Immunol. **9**:431–455.
30. **Lövkvist, L., H. Sjölinder, R. Wehelie, H. Aro, A. Norrby-Teglund, L. Plant, and A.-B. Jonsson.** 2008. CD46 contributes to the severity of group A streptococcal infection. Infect. Immun. **76**:3951–3958.
31. **Manchester, M., M. K. Liszewski, J. P. Atkinson, and M. B. Oldstone.** 1994. Multiple isoforms of CD46 (membrane cofactor protein) serve as receptors for measles virus. Proc. Natl. Acad. Sci. USA **91**:2161–2165.
32. **Medina, E., O. Goldmann, A. W. Toppel, and G. S. Chhatwal.** 2003. Survival of *Streptococcus pyogenes* within host phagocytic cells: a pathogenic mechanism for persistence and systemic invasion. J. Infect. Dis. **187**:597–603.
33. **Miyoshi-Akiyama, T., J. Zhao, K. Kikuchi, H. Kato, R. Suzuki, M. Endoh, and T. Uchiyama.** 2003. Quantitative and qualitative comparison of virulence traits, including murine lethality, among different M types of group A streptococci. J. Infect. Dis. **187**:1876–1887.
34. **Mrkic, B., J. Pavlovic, T. Rülicke, P. Volpe, C. J. Buchholz, D. Hourcade, J. P. Atkinson, A. Aguzzi, and R. Cattaneo.** 1998. Measles virus spread and pathogenesis in genetically modified mice. J. Virol. **72**:7420–7427.
35. **Naniche, D., G. Varior-Krishnan, F. Cervoni, T. F. Wild, B. Rossi, C. Rabourdin-Combe, and D. Gerlier.** 1993. Human membrane cofactor protein (CD46) acts as a cellular receptor for measles virus. J. Virol. **67**:6025–6032.
36. **Nizet, V., T. Ohtake, X. Lauth, J. Trowbridge, J. Rudisill, R. A. Dorschner, V. Pestonjamasp, J. Piraino, K. Huttner, and R. L. Gallo.** 2001. Innate antimicrobial peptide protects the skin from invasive bacterial infection. Nature **414**:454–457.
37. **Okada, N., M. K. Liszewski, J. P. Atkinson, and M. Caparon.** 1995. Membrane cofactor protein (CD46) is a keratinocyte receptor for the M protein of the group A streptococcus. Proc. Natl. Acad. Sci. USA **92**:2489–2493.
38. **Peyssonnaux, C., A. S. Zinkernagel, V. Datta, X. Lauth, R. S. Johnson, and V. Nizet.** 2006. TLR4-dependent hepcidin expression by myeloid cells in response to bacterial pathogens. Blood **107**:3727–3732.
39. **Rezcallah, M. S., K. Hodges, D. B. Gill, J. P. Atkinson, B. Wang, and P. P. Cleary.** 2005. Engagement of CD46 and α5β1 integrin by group A streptococci is required for efficient invasion of epithelial cells. Cell. Microbiol. **7**:645–653.
40. **Santoro, F., P. E. Kennedy, G. Locatelli, M. S. Malnati, E. A. Berger, and P. Lusso.** 1999. CD46 is a cellular receptor for human herpesvirus 6. Cell **99**:817–827.
41. **Segerman, A., J. P. Atkinson, M. Marttila, V. Dennerquist, G. Wadell, and N. Arnberg.** 2003. Adenovirus type 11 uses CD46 as a cellular receptor. J. Virol. **77**:9183–9191.
42. **Sjolinder, H., and A. B. Jonsson.** 2007. Imaging of disease dynamics during meningococcal sepsis. PLoS ONE **2**:e241.
43. **Sjölinder, H., L. Lövkvist, L. Plant, J. Eriksson, H. Aro, A. Jones, and A.-B. Jonsson.** 2008. The ScpC protease of *Streptococcus pyogenes* affects the outcome of sepsis in a murine model. Infect. Immun. **76**:3959–3966.
44. **Stefanini, M., C. De Martino, and L. Zamboni.** 1967. Fixation of ejaculated spermatozoa for electron microscopy. Nature **216**:173–174.
45. **Sumby, P., A. R. Whitney, E. A. Graviss, F. R. DeLeo, and J. M. Musser.** 2006. Genome-wide analysis of group A streptococci reveals a mutation that modulates global phenotype and disease specificity. PLoS Pathog. **2**:e5.
46. **Tewodros, W., and G. Kronvall.** 2005. M protein gene (*emm* type) analysis of group A beta-hemolytic streptococci from Ethiopia reveals unique patterns. J. Clin. Microbiol. **43**:4369–4376.
47. **Walker, M. J., A. Hollands, M. L. Sanderson-Smith, J. N. Cole, J. K. Kirk, A. Henningham, J. D. McArthur, K. Dinkla, R. K. Aziz, R. G. Kansal, A. J. Simpson, J. T. Buchanan, G. S. Chhatwal, M. Kotb, and V. Nizet.** 2007. DNase Sda1 provides selection pressure for a switch to invasive group A streptococcal infection. Nat. Med. **13**:981–985.
48. **Wu, E., S. A. Trauger, L. Pache, T.-M. Mullen, D. J. von Seggern, G. Siuzdak, and G. R. Nemerow.** 2004. Membrane cofactor protein is a receptor for adenoviruses associated with epidemic keratoconjunctivitis. J. Virol. **78**: 3897–3905.

Editor: J. N. Weiser

doi:10.1016/j.jmb.2007.08.024 J. Mol. Biol. (2007) 373, 1089–1097

JMB

Available online at www.sciencedirect.com

ScienceDirect

ELSEVIER

COMMUNICATION

Crystal Structure of *Streptococcus dysgalactiae*-Derived Mitogen Reveals a Zinc-Binding Site and Alterations in TcR Binding

Susanna Saarinen[1], Hidehito Kato[2], Takehiko Uchiyama[2], Tohru Miyoshi-Akiyama[3] and Anastassios C. Papageorgiou[1]*

[1]*Turku Center for Biotechnology, University of Turku and Åbo Akademi University, PO Box 123, Tykistökatu 6, BioCity, Turku 20521, Finland*

[2]*Department of Microbiology and Immunology, Tokyo Women's Medical University, 8-1 Kawada-cho, Shinjuku-ku, Tokyo 162-8666, Japan*

[3]*Department of Infectious Diseases, Research Institute, International Medical Center of Japan, 1-21-1, Toyama, Shinjuku-ku, Tokyo 162-8655, Japan*

Received 31 May 2007; received in revised form 13 August 2007; accepted 14 August 2007
Available online 21 August 2007

Edited by R. Huber

Bacterial superantigens are protein toxins with an ability to cause serious diseases in humans by activating a large number of T cells. *Streptococcus dysgalactiae*-derived mitogen (SDM) is a novel superantigen that is distinct from other known superantigens based on phylogenetic analysis. The X-ray structure of SDM has been determined at 1.95 Å resolution. SDM shares the same characteristic fold with other superantigens, but it shows a major structural difference due to the lack of the α5 helix between the β10 and β11 strands. A bound zinc ion was identified in the structure at the C-terminal domain of the molecule. SDM appears to bind to the major histocompatibility complex class II β-chain through the zinc-binding site, as described by mutagenesis data and structural comparisons. T-cell binding instead shows a significant difference compared to other superantigens. The mutation of Asn11 (a conserved residue that is known to be significant for T-cell-receptor binding in other superantigens) and Lys15 to Ala did not cause any decrease in the mitogenic activity of SDM. This observation and the lack of the α5 helix suggest alterations in T-cell-receptor binding.

Keywords: superantigens; *Streptococcus*; immunomodulation; T-cell receptor; zinc binding

Introduction

Superantigens are a group of proteins that are able to cause a massive T-cell expansion. A large number of superantigens from different bacteria and viruses are now known.[1] All superantigens share an ability to cross-link major histocompatibility complex class II (MHCII) molecules with T-cell receptors (TcRs). Superantigens bind directly to invariant regions of MHCII molecules outside the classical antigen-binding groove without being preprocessed in the cell, in contrast to conventional antigens. A conventional antigen presented to a TcR by an MHCII molecule activates 0.01–0.0001% of resting T cells, while superantigens are able to activate 10–30% of T cells. This makes superantigens the most powerful T-cell mitogens to have ever been discovered.

*Corresponding author. E-mail address: tassos.papageorgiou@btk.fi.

Abbreviations used: MBP, myelin basic protein; MHCII, major histocompatibility complex class II; SDM, *Streptococcus dysgalactiae*-derived mitogen; SE, staphylococcal enterotoxin; SPE, streptococcal pyrogenic exotoxin; TcR, T-cell receptor.

Superantigen-induced T-cell activation leads to an extensive production of inflammatory cytokines, such as tumor necrosis factors α and β, and interleukin-2.[2–4] This can result in acute diseases, including toxic shock syndrome and food poisoning. There are also indications that superantigens are implicated in chronic and autoimmune diseases such as Kawasaki disease, rheumatoid arthritis, and diabetes.[5]

The number of known superantigens has increased significantly over the past years. The best-characterized members of the superantigen family are staphylococcal enterotoxins (SEs), which are secreted by *Staphylococcus aureus*, and streptococcal pyrogenic exotoxins (SPEs), which are secreted by *Streptococcus pyogenes*. Other Gram-positive or Gram-negative bacteria, such as *Yersinia pseudotuberculosis*, mycoplasmata, and viruses, can also produce superantigens. Although the sequence identities of characterized superantigens range from 18% to almost 100%, structural studies have shown that superantigens share a similar fold that consists of an N-terminal β-barrel and a C-terminal β-grasp domain separated by a long central α-helix.[2] The crystal structures of many superantigens have been resolved. In addition, several superantigen/MHCII[6–9] and superantigen/TcR Vβ-chain complexes have been structurally determined.[10–12]

Superantigen binding to MHCII molecules can occur in three distinct ways: (i) through the α-chain of the MHCII molecule; (ii) through the β-chain; and (iii) through both chains. The binding sites for the α- and β-chains are located at opposite sites of the superantigen molecule. Binding to the MHCII β-chain requires the presence of a zinc ion ligated by three residues from the C-terminal domain of the superantigen molecule.[13] His81 of the MHCII β-chain[14–16] is the fourth ligand to result in a tetrahedrally coordinated zinc ion. This binding mode has a stronger affinity than the one through the α-chain.

Different superantigens show striking differences in binding modes and in affinities to different TcR Vβ-chains.[1,4] The complementarity-determining regions 1–3, the third framework region, and the fourth hypervariable loop of the TcR Vβ-chain can interact with superantigens. The number of contacts and contact areas differs for each superantigen. Hydrogen bonds ordinarily involve only the main-chain atoms of the TcR Vβ-chain, which make side-chain variations less likely to affect the binding affinity. However, the crystal structure of SPE-C, in complex with Vβ2.1, showed also side-chain atoms from the Vβ-chain to be involved in binding.[11]

Streptococcus dysgalactiae belongs to the C/G Lancefield group of streptococci, which have been found to cause infections similar to those of *S. pyogenes*.[17] *Streptococcus dysgalactiae*-derived mitogen (SDM) is a superantigen purified from *S. dysgalactiae* culture supernatant.[18] The pathogenic role of this superantigen in infections is not known. SDM has been shown to activate T cells with Vβ1 and Vβ23 variable regions. The mature protein (25 kDa) is composed of 212 amino acids. SDM shows an approximately 30% homology with other superantigens at the amino acid sequence level. Phylogenetic analysis indicates that SDM belongs to a family that is distinct from other known bacterial superantigens.[18] This family also includes SPE-L (with 58% identity and 74% similarity with SDM) and SPE-M (with 98% identity). Moreover, recent studies have classified SDM as belonging to group IV superantigens[19] where it forms a separate subbranch.[20]

Here, we present the crystal structure of SDM at 1.95 Å resolution as the first representative of the new superantigen subbranch in group IV. The structure has revealed the presence of a zinc-binding site and alterations in secondary structure elements. Detailed comparisons with the crystal structures of other superantigens were performed. A zinc-mediated binding mode for MHCII molecules was proposed after mutagenesis experiments and comparisons with superantigen/MHCII complexes had been performed. Furthermore, the SDM structure was compared to superantigen/TcR Vβ-chain complexes, and mutagenesis experiments were performed to enlighten SDM binding to the Vβ-chain.

Quality of the structure

The crystal structure of SDM was determined by molecular replacement and refined at 1.95 Å resolution. The final R_{cryst} is 20.8%, with an R_{free} of 24.1%. The average *B*-factor is 41.7 Å^2. Data collection and refinement statistics are summarized in Table 1. The Ramachandran plot showed that 91.3% of

Table 1. Data collection and refinement statistics

Data processing	
Space group	$P3_2$
Cell dimensions	
a, *b*, *c* (Å)	51.9, 51.9, 62.1
β (°)	120
Resolution range (Å)	99–1.95 (1.98–1.95)
Number of observations	101,908
Number of unique reflections	13,696
Completeness (%)	96.3 (90.8)
R_{sym} (%)	4.8 (42.0)
$\langle I/\sigma(I)\rangle$	21.2 (2.5)
Number of molecules (a.u.)	1
Refinement statistics	
Resolution range (Å)	40.0–1.95
Number of reflections (working set/test set)	12,447/672
R_{cryst}/R_{free} (%)	20.8/24.1
Protein atoms	1601
Water molecules	93
Glycerol molecules	2
RMSD	
Bond length (Å)	0.010
Bond angle (°)	1.47
Average *B*-factors (Å^2)	
Main chain	40.9
Side chain	42.5
Water molecules	41.7
Glycerol molecules	66.1
Zinc	51.3
Wilson *B*-factor	36.3

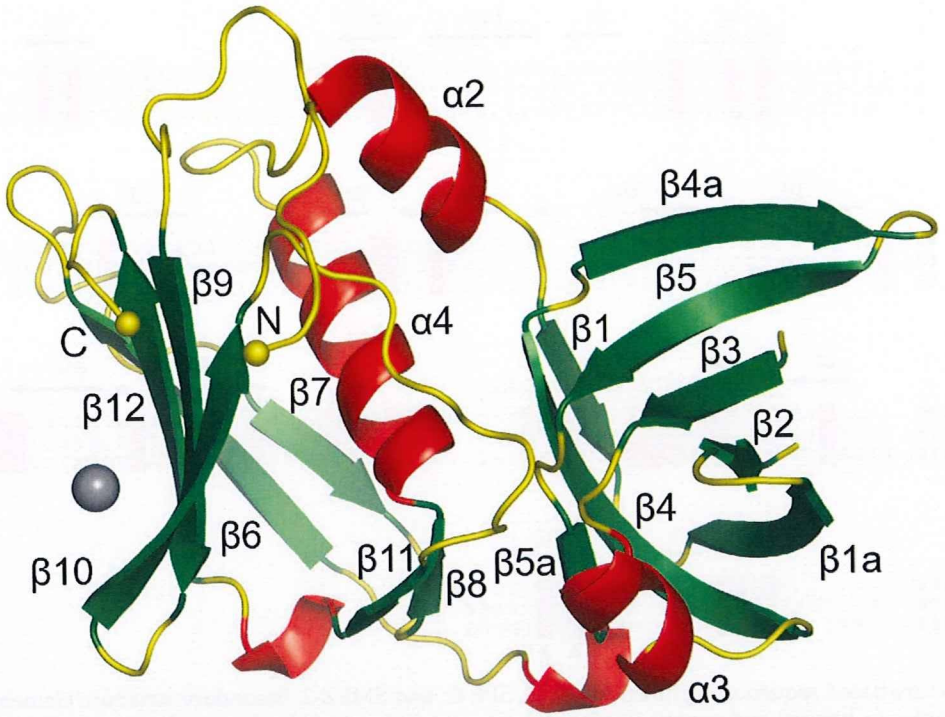

Fig. 1. Cartoon representation of SDM. The N- and C-termini are shown as small spheres. Helices are depicted in red, and β-strands are depicted in green. The zinc ion is shown as a gray sphere.

nonproline and nonglycine residues are in the most favoured regions, as defined in PROCHECK,[21] and none is in disallowed regions. The final model includes 195 residues (residues 1–36 and 51–209) out of 212 residues in the complete SDM sequence. No density could be seen for the region between residues 36 and 51. This region of the structure is solvent-exposed and presumably highly flexible. A codon encoding for an additional residue (Lys0) was inserted into the N-terminus of the *sdm* gene in the expression construct to facilitate the removal of the His tag, and density for Lys0 was detected. The last three C-terminal residues were not modelled due to lack of density. Side-chain density was not detected for residues Glu8, Lys27, Ser99, Gln116, Lys120, Lys126, Asn151, and Ile161; thus, they are presented as alanines in the final structure.

Overall description

SDM shares the overall fold of superantigens characterized by a trapezoid shape and closely packed N- and C-terminal domains (Fig. 1). The N-terminal domain forms a β-barrel of five mixed β-strands. The C-terminal domain has a β-grasp fold in which the α4 helix (residues 136–149) is packed against a mixed β-sheet of five strands, β6, β7, β9, β10, and β12. SDM has two cysteines (residues 84 and 162), which are distant from each other (approximately 43 Å) and do not form a disulphide bridge. Cys84 is located in the loop between the β4 and β5 strands in the periphery of the molecule. This particular location may create a possibility for Cys84 to form a sulphur bridge with a similar cysteine from another SDM molecule. It has been observed earlier that solvent-exposed Cys90 residues of a SPE-A dimer are capable of forming an intermolecular disulphide bridge.[22] SPE-A Cys90 is located in a similar kind of a loop as SDM Cys84, and this could indicate that SDM may form a dimer under different crystallization conditions. Cys162 of SDM is buried; hence, it cannot form an intermolecular disulphide bond.

Structural comparisons with other superantigens

SDM was structurally compared with other superantigens using SSM†. SDM showed a 32% sequence identity with SPE-C (Protein Data Bank entry 1AN8) and a 28% sequence identity with SMEZ-2 (1EU3) (Fig. 2). The root-mean-square deviations (RMSDs) in Cα positions are 1.54 and 1.92 Å, respectively. The greatest structural difference is the lack of the α5 helix in the SDM structure between the β10 and β11 strands (Fig. 3). Other superantigens that are known to share a similar gap with SDM in the amino acid sequence around the region forming the α5 helix and the part of the loop between the α5 helix and the β10 strand are SPE-L and SPE-M.[23] Therefore, SPE-L and SPE-M are expected to share a similar geometry in that region. This structural difference can also cause changes in the binding of other proteins, such as MHCII and TcR. Apart from that difference, other structural variations are minor and placed on surface areas of the molecule.

† www.ebi.ac.uk/msd-src/ssm/

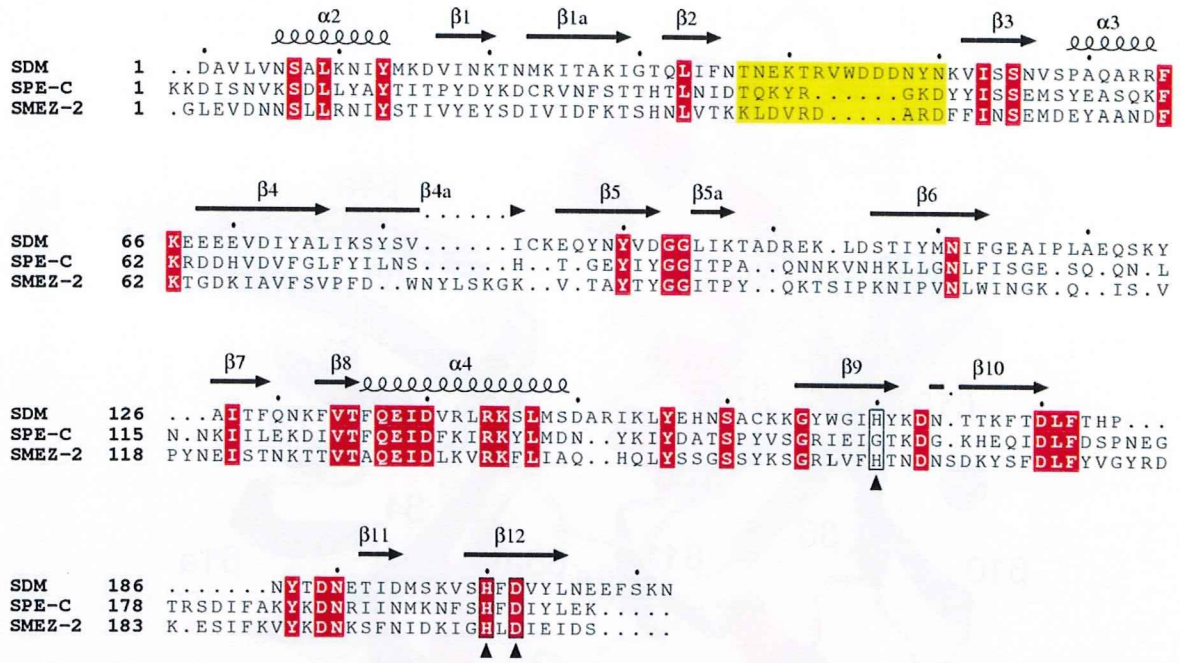

Fig. 2. Structure-based sequence alignment of SDM, SPE-C, and SMEZ-2. Secondary structure elements for SDM are shown as squiggles (α-helices) and arrows (β-strands). Characters on a red background are conserved. Black triangles show zinc-binding residues of SDM. Characters on a yellow background are not structurally aligned due to a gap in the SDM crystal structure. Every 10th residue of SDM is shown with a black dot.

Superantigens have conserved amino acids and regions. Comparisons between superantigen structures have revealed that the region consisting mainly of the α2 and α4 helices and connecting the N- and C-terminal domains is conserved in most superantigens. In particular, the α4 helix is highly conserved, and it appears that SDM can form most of the hydrogen bonds in this region similarly to other superantigens despite the fact that it lacks the α5 helix (Table 2). SDM also shares several conserved residues, such as Tyr13, Gly94, and Tyr189 (which are all shown to form hydrogen bonds combining N- and C-terminal parts), and Leu147 in the hydrophobic core of the C-terminus.

This conserved region includes two salt bridges in SMEZ-2, which are also seen in other superantigens.[24] SDM can form a salt bridge between residues Asp140 and Arg144, which is analogous to the Asp134–Arg138 salt bridge of SMEZ-2. However, a salt bridge found in SMEZ-2 between Lys125 and Glu132 cannot be formed in SDM because SDM has an uncharged residue (Asn131), instead of a lysine residue, at the location equivalent to SMEZ-2 Lys125. The side chains of Asn131 and Glu138 in SDM are also too distant (>6 Å) from each other to form a hydrogen bond. The presence of lysine in position 131 of SDM appears to be sterically forbidden due to potential clash with the side chain of the nearby Arg101.

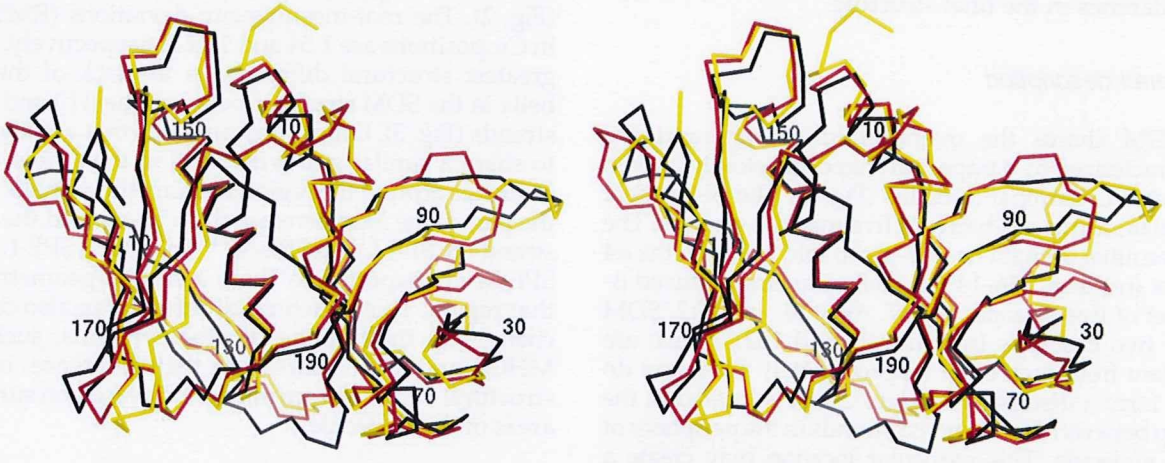

Fig. 3. Cα atom stereodiagram of SDM superimposed onto SPE-C and SMEZ-2. SDM, black; SPE-C, red; SMEZ-2, yellow.

Table 2. Globally conserved intramolecular hydrogen bonds in SDM and SMEZ-2

	Residue (atom)	Residue (atom)	Distance (Å)
SDM	Tyr13 (OH)	Tyr187 (OH)	2.81
SMEZ-2	Tyr13 (OH)	Tyr189 (OH)	2.82
SDM	Asp92 (O)	Gln137 (NE2)	2.88
SMEZ-2	Tyr88 (O)	Gln131 (NE2)	3.87
SDM	Gly94 (N)	Asn190 (OD1)	2.90
SMEZ-2	Gly90 (N)	Asn192 (OD1)	2.82
SDM	Thr135 (OG1)	Glu138 (N)	3.19
SMEZ-2	Thr129 (OG1)	Glu132 (N)	2.98
SDM	Asp140 (OD2)	Tyr187 (OH)	2.62
SMEZ-2	Asp134 (OD2)	Tyr189 (OH)	2.53
SDM	Arg144 (NH1)	Tyr156 (OH)	2.99
SMEZ-2	Arg138 (NH1)	Tyr148 (OH)	2.92

Zinc-binding site

Several superantigens are able to bind to the MHCII β-chain through a zinc ion. During the refinement of the SDM structure, a spherical electron density was identified at ~14σ on the difference electron density map and in a location similar to that of the zinc-binding sites in other superantigen structures. Anomalous data collected at the zinc absorption edge showed a density visible at ~30σ on the calculated anomalous difference map (Fig. 4). Further confirmation of the presence of zinc came through direct coupled plasma analysis (Spectra-Span 7 spectrometer; ARL-Fisons Instruments USA). Based on the surrounding residues and element analysis, a zinc atom was placed and subsequently refined to a *B*-factor of 51.1 Å^2. The zinc-binding site of SDM consists of His170, from the β9 strand, and His200 and Asp202, both from the β12 strand. The zinc-binding atoms are ND1 of His170, NE2 of His200, and OE2 of Asp202. This makes the SDM zinc-binding site analogous to the zinc-binding site of SMEZ-2 (His162, His202, and Asp204).[22,23] Compared to the zinc-binding site of SPE-C,[25] SDM His170 and SPE-C His167 are located in different β-strands, although the other ligands are equivalent. Interestingly, SDM His170 is structurally aligned to a Gly residue in SPE-C, hence explaining the use of a His residue from a neighbouring β-strand in SPE-C. No fourth ligand was found for the zinc in SDM. Inspection of the symmetry-related molecules showed that none of them makes crystal contacts with the zinc ion (Table 3).

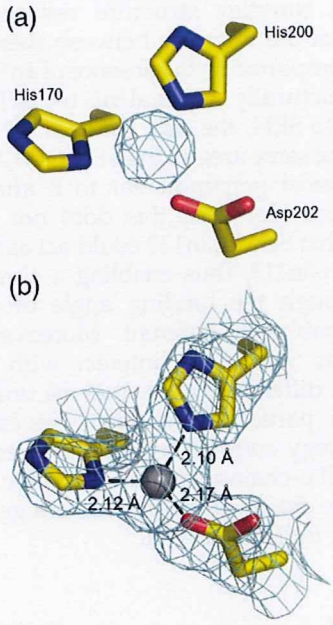

Fig. 4. The zinc-binding site of SDM. (a) Difference electron density map based on anomalous scattering. (b) The zinc-binding site of SDM on the final $2|F_o|-|F_c|$ electron density map.

The metal–ligand distances (2.12 Å for His170, 2.10 Å for His200, and 2.17 Å for Asp202) are longer than those expected for ideal zinc binding, possibly due to a low crystallization pH (4.2). It has been suggested that the low pH level can cause an increase in coordination distances.[26] Another (and more probable) explanation for this increase is that the precision of bond lengths is good only at very-high-resolution protein structures, and this can allow higher variations in bond lengths.[27] Although histidines are expected to be protonated at pH values lower than 6.0 (a condition that could cause the removal of zinc),[26] zinc is still present despite the low crystallization pH.

MHCII-binding site

In order to determine potential MHCII-binding sites in SDM, the latter was superimposed structurally onto SEB/HLA-DR1,[6] SPE-C/myelin basic protein (MBP) peptide/HLA-DR2a,[7] and SEH/haemagglutinin (HA) peptide/HLA-DR1[8] complexes. In the first complex, the superantigen binds directly to the MHCII α-chain, while in the other complexes, binding is mediated through the β-chain of the MHCII molecule.

Table 3. Major intermolecular contacts

Source atom	Target atom	Distance (Å)
Asp1 OD1	Lys20 NZ	2.66
Ala2 N	Asn19 O	3.18
Val3 O	Gln130 NE2	3.01
Asp16 OD1	Asn56 ND2	3.19
Lys20 NZ	GOL501 O2	3.07
Thr21 N	Lys0 O	2.78
	Lys0 CG	3.06
	Lys0 N	2.87
Lys51 NZ	GOL501[a] O3	2.45
Asn56 ND2	Wat76	3.12
Arg64 NH2	Gly114 O	3.10
Glu68 CD	Asp105 OD2	3.08
OE1		2.65
Lys85 NZ	Tyr166 OH	2.40
	Glu207 OE1	2.47
Gln87 NE2	Wat72	2.65
Asp100 OD1	Pro118 CA	3.02
	Leu119 N	3.03
Glu102 OE2	Glu67 OE1	2.82
Gln130 NE2	Wat87	3.20

Cutoff limits, 2.3–3.2 Å.
[a] Glycerol 501.